Physics – Uspekhi **53** (7) 645 – 675 (2010)

REVIEWS OF TOPICAL PROBLEMS PACS numbers: 03.65.Ge, **28.20.–v**, 29.30.Hs

Near-surface quantum states of neutrons in the gravitational and centrifugal potentials

V V Nesvizhevsky

DOI: 10.3367/UFNe.0180.201007a.0673

Contents

Abstract. Two related physical phenomena have recently been observed: quantum states of ultracold neutrons (UCN) in the gravitational field above a flat mirror, and quantum states of cold neutrons (CN) in an effective centrifugal potential in the vicinity of a concave mirror. The two phenomena are similar in terms of their associated experimental methods and mathematical representations as well as in terms of their applications in particle physics, quantum optics, and surface physics.

1. Introduction

If we raise a ping-pong ball to a height H_0 above a table and let it gently drop, the ball accelerates in Earth's gravity field to the velocity $V_0 = \sqrt{2gH_0}$, where $g \approx 9.81$ m s^{-1} is the gravitational acceleration, and is then reflected from the table surface. In the case of a perfectly elastic reflection in a vacuum, the ball would return due to gravity to the surface after the time interval $\Delta\tau_0(H_0) = \sqrt{8H_0/g}$ and would then continue bouncing with the frequency $\nu_0(H_0) = 1/\tau_0(H_0) = \sqrt{g/(8H_0)}$. The smaller H_0 is, the larger ν_0: $\nu_0\,(1\,\text{m}) \approx 1$ Hz, $\nu_0\,(1\,\text{cm}) \approx 10$ Hz, $\nu_0\,(100\,\mu\text{m}) \approx 10^2$ Hz, as follows from the equality of the maximum potential and kinetic energies of the ball: $MV_0^2/2 = MgH_0$. The frequency ν_0 is independent of the ball mass M.

We consider another experiment (Fig. 1). A table is moving together with a spaceship with the acceleration $\mathbf{a} = -\mathbf{g}$ far from large gravitating masses. The table surface is perpendicular to $\mathbf{g}$. An observer in the spaceship sees the ball bouncing on the table with the same frequency as in the previous experiment (neglecting the small inhomogeneity of the gravitational field). But a rest-frame observer sees the table in the spaceship accelerating toward the ball. This is a consequence of the weak equivalence principle, which has been verified with the amazing accuracy $\sim 10^{-12}$ for macroscopic objects [1], and with the accuracy $\sim 3 \times 10^{-4}$ for classical elementary particles [2]. We note that the unavoidable small inhomogeneity of the gravitational field causes

V V Nesvizhevsky European Center of Neutron Investigations, Institut Laue–Langevin, 6 rue Jules Horowitz, F-38042 Grenoble, France
Tel. +(33) -476207795. Fax +(33) -476207777
E-mail: nesvizhevsky@ill.eu

Received 6 November 2009
Uspekhi Fizicheskikh Nauk **180** (7) 673 – 707 (2010)
DOI: 10.3367/UFNr.0180.201007a.0673
Translated by V V Nesvizhevsky; edited by A M Semikhatov

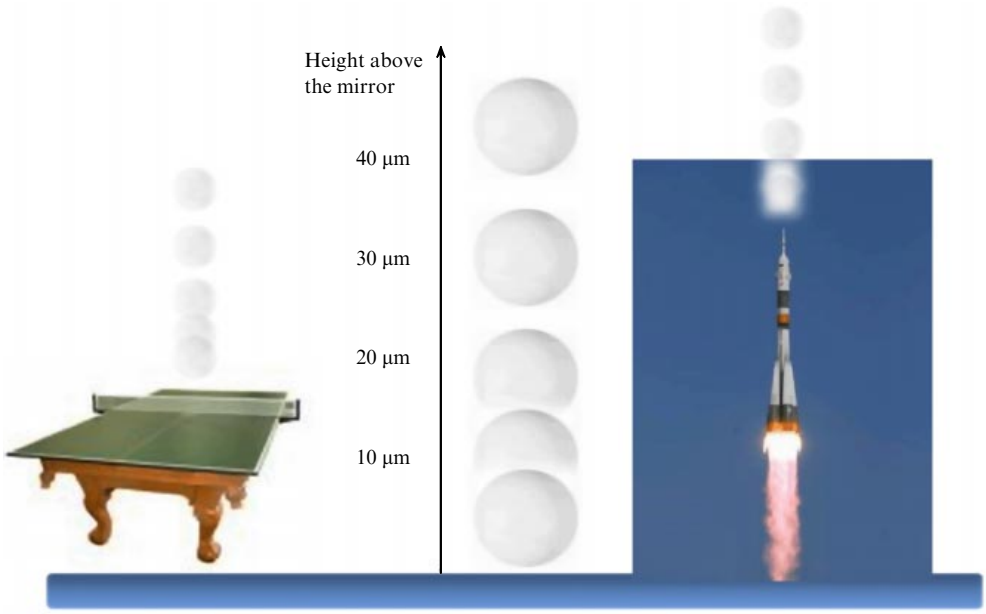

Figure 1. The quantum behavior of an object above a mirror in the gravity field and in an accelerating reference frame is illustrated schematically. The ball heights correspond to its most probable positions; the scale corresponds to the neutron mass; we consider the 5th quantum state.

interesting observable quantum effects; we will consider them in a separate work.

What would happen in these two experiments at very small heights H? Would these two problems still be equivalent in the quantum limit? Would the frequency v_0 tend to infinity? No, it would increase as long as H_0 exceeds the quantum mechanical limit H_0^{QM}, which can be estimated using the Heisenberg position–momentum uncertainty relation

$$H_0^{\mathrm{QM}} M\sqrt{2gH_0^{\mathrm{QM}}} \approx 2\pi\hbar\,,$$

where $\hbar$ is the Planck constant. For a ball in Earth's gravitational field, the height $H_0^{\mathrm{QM}} \approx 10^{-21}$ m is too small, and quantum phenomena cannot be observed, but for an elementary particle above a mirror, for instance, for an ultracold neutron (UCN) [3–5] with the mass $m \approx 1$ GeV, quantum effects can be observed at relatively large heights $H_0^{\mathrm{QM}} \approx 10$ μm [6, 7]. A mirror for UCNs can be provided by the optical potential [8] of a polished solid surface or liquid [2] due to the neutron–nucleus interaction; also, a mirror can be formed by the magnetic field gradient interacting with the neutron magnetic moment [9]. Similar measurements can be carried out using ultracold atoms [10, 11]. A mirror for atoms can be built using a one-dimensional surface light wave [12–14] or magnetic field gradient [15]. The condition separating the quantum and classical behavior of UCNs above a mirror is defined by the ratio of the neutron quantum state width δE_n (the reciprocal neutron lifetime τ_n^{-1} in the nth quantum state) and the energy difference between neighboring quantum states $\Delta E_{n+1,n} = E_{n+1} - E_n$ (i.e., the energy–time uncertainty relation $\tau_n \Delta E_{n+1,n} \approx 2\pi\hbar$). Low quantum states can be resolved under certain conditions, while particles with larger energies (velocities) form a classical continuum. The transition from classical to quantum behavior of a massive particle above a mirror is considered, e.g., in Refs [16, 17]. The authors also discuss analogous experiments with larger objects, like fullerenes.

In the quantum limit, we do not consider trajectories, heights, or velocities; the frequency is defined by the object energy as $v_0^{\mathrm{QM}} \approx E_0/(2\pi\hbar)$, and the characteristic height H_0^{QM} depends on the object mass. In accordance with the weak equivalence principle, the effective centrifugal potential [18] is locally equivalent to gravity. Therefore, objects do not fall in a gravitational field and do not move in accelerated reference frames universally: although massive objects behave classically, light objects exhibit quantum properties at equal distances to the mirror. In other words, by measuring the parameters of a ball bouncing on a surface (the parameters of its quantum states), we can calculate the ball mass. Hence, the classical statement on the universality of free fall, i.e., on its independence of mass, is not valid in the quantum limit. But the general relativity weak equivalence principle (assuming the local equivalence of gravity and acceleration) is valid. In our case, this means that the quantum states of neutrons in gravitational and centrifugal potentials are equivalent if the accelerations are equal.

The general solution of the Schrödinger equation describing a particle bouncing on a mirror due to an attractive linear potential was found in the 1920s [19]. But this problem was long considered to be nothing more than a good exercise in textbooks on quantum mechanics [20–26]. Nevertheless, conditions corresponding to this idealized problem were realized recently in experiments with ultracold neutrons in a gravity field [27–29] and with cold neutrons (CNs) in a centrifugal effective potential [18, 30, 31] (see also Ref. [32]) at the European neutron center, Institut Laue–Langevin (ILL), Grenoble, France, in which Russia had participated until recently. A theoretical analysis of these experiments, as well as related additional information and reviews on this subject can be found in Refs [33–50].

It is curious that the measurement of neutron quantum states in gravitational and centrifugal potentials is the first direct demonstration of the weak equivalence principle of general relativity for an object (particle) in a quantum state. As we show in what follows, these phenomena constitute an excellent laboratory for measuring quantum optics phenomena, localization, interference, and their applications to various domains of physics. Gravitational quantum states of

UCNs provide a unique opportunity to study a interactions of quantum systems with a gravitational field. Experiments using configurations analogous to those used in (or planned for) neutron experiments described in this review are considered in relation to ultracold atoms, e.g., in Refs [51, 52]. The gravitational properties of antimatter could probably be studied in measurements of quantum reflection of ultracold antihydrogen atoms from a horizontal material surface [53, 54] in similar geometry. If we replace the gravitational potential with an electromagnetic attractive potential, the problem of a particle bouncing on a mirror describes electrons levitating above a superliquid helium surface in an attractive linear electric potential [55], or polarized hydrogen atoms levitating in a magnetic field gradient [56]. An optical model of our phenomenon is, to some extent, given by light propagation through a cylindrically shaped set of thin light guides as described in Ref. [57]. Other configurations of experiments with neutrons involving quantum effects caused by gravity can also be considered [58, 59].

This review is organized as follows.

Section 2 presents a theoretical treatment of nonperturbed gravitational quantum states of UCNs above an ideal mirror, and a general analysis of the feasibility of the experimental observation of such states. We list the properties of UCNs important for the presented experiments.

In Section 3, we discuss two methods of observation of gravitational quantum states of UCNs. The integral flow-through method amounts to measuring the UCN flux through a narrow slit between a horizontal mirror and a flat scatterer/absorber above it (we call it a scatterer in what follows). We consider theoretical models describing neutron interaction with a scatterer. We show that the tunneling of neutrons through a gravitational barrier separating classically allowed heights for a UCN and a scatterer is the decisive factor. The differential observation method assumes direct measurement of neutron wave functions using position-sensitive UCN detectors of high spatial resolution developed for this particular experiment.

Section 4 describes the main results of measurements of neutron gravitational quantum states. In the first series of experiments, the integral method was used. It allowed identifying the discrete behavior of the neutron flux above a mirror corresponding to the lowest quantum state. Thus, the existence of the phenomenon itself was proven. Systematic effects that can affect this conclusion are analyzed. In the second series of experiments, spectrometer parameters were improved significantly, the number of statistics were increased, and the possible systematic effects were analyzed in detail using experimental and theoretical methods. These experiments also allowed identifying the first 'excited' quantum state. Finally, experiments with position-sensitive UCN detectors of high spatial resolution proved the feasibility of observing UCN gravitational quantum states using the differential method.

The prospects for increasing accuracy in measurements of quantum state parameters are considered in Section 5. The major factors are the long-term storage of neutrons in quantum states and the maximum populations of quantum states. The latter is defined by the initial density of UCNs in the phase space and by the efficient delivery of UCNs to the spectrometer. Particular attention is given to the feasibility of measuring resonant transitions between quantum states. Quantum transitions can be induced by strong nuclear, magnetic, and eventually even gravitational interaction. Besides, we can study oscillations between states in the absence of any interactions mixing them. The simultaneous use of two methods to induce the resonant transition (for instance, intense magnetic plus weak gravitational perturbations) and the observation of interference between the amplitudes of these transitions increase the sensitivity to the weaker interaction.

The range of applications of neutron gravitational states and related methods developed within the current scientific program is rapidly broadening. In Section 6, we consider applications of this phenomenon to particle physics for searching for additional fundamental short-range interactions or exotic particles, for constraining the neutron electric charge, for measuring quantum optics phenomena, and for studying interactions of neutrons in quantum states with a gravitational field. In this and other sections, we mention methodical applications of UCN gravitational quantum states and applications of spectrometers, such as measurements of surface layers, efficient neutron transport, in particular, angular-selective extraction of neutrons from UCN sources, and traps with no significant loss of phase-space density.

Section 7 briefly describes the first observation of neutron quantum states in an effective centrifugal potential in the vicinity of a curved mirror.

2. Quantum states of ultracold neutrons (UCNs) in a gravitational field

The Schrödinger equation for the problem of UCNs above a mirror in an attractive linear potential is solved in Section 2.1. Section 2.2 describes the UCN properties that are important for the presented experiments.

2.1 The problem of UCN quantum states above a mirror in a gravitational field

The neutron wave function $\psi(z)$ in Earth's gravitational field above a mirror is governed by the Schrödinger equation

$$\frac{\hbar^2}{2m}\frac{\mathrm{d}^2\psi(z)}{\mathrm{d}z^2} + (E - mgz)\,\psi(z) = 0\,. \qquad (1)$$

An ideal horizontal mirror at the height $z = 0$ can be approximated as an infinitely high and abrupt potential step; this approximation is justified by characteristic values of energies and lengths in our problem. The energy of neutrons in low quantum states, $\sim 10^{-12}$ eV, is much smaller than the optical potential of the mirror material, $\sim 10^{-7}$ eV, and the characteristic range of increase in the optical potential for a polished mirror, $\sim 10^{-9}$ m, is much smaller than the wavelength of neutrons in low quantum states, $\sim 10^{-5}$ m. Such an infinitely high and abrupt optical potential corresponds to the zero boundary condition for the wave function, $\psi(z = 0) = 0$. A solution of the Schrödinger equation can be written in terms of the Airy function $\psi(z) = C\,\mathrm{Ai}(z/z_0)$, where $z_0 = [\hbar^2/(2m^2g)]^{1/3} = 5.87$ μm is the characteristic length scale of the problem and C is a normalization constant. The Airy function zeros λ_n define quantum state energies $E_n = mgz_0\lambda_n$; $\varepsilon_0 = mgz_0 = 0.602$ peV is the characteristic energy of the problem and $f_0 = \varepsilon_0/(2\pi\hbar) = 145$ Hz is its characteristic frequency. For the four lowest states, the zeros of the Airy function are $\lambda_n = \{2.34, 4.09, 5.52, 6.79\ldots\}$. The eigenfunctions of the quan-

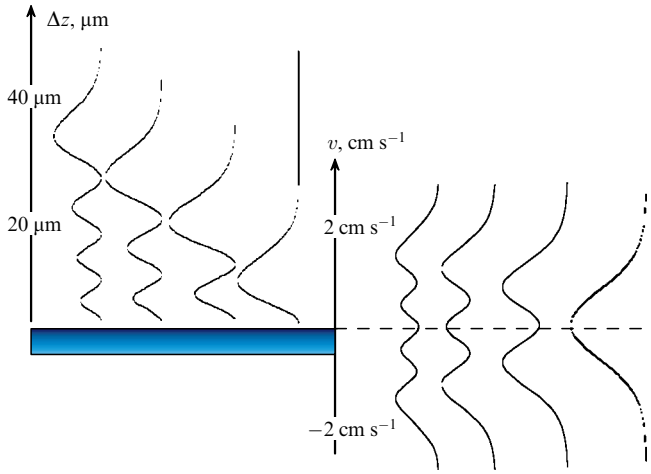

Figure 2. Squared moduli of the neutron wave functions $|\psi_n(z)|^2$ are shown on the left as a function of the height z for the four lowest quantum states; they correspond to the probabilities of observing neutrons. Squared moduli $|\phi_n(v)|^2$ are shown on the right as a function of the velocity v for these quantum states; they provide the probabilities of observing the neutron velocity v.

tum states are

$$\psi_n\big(\xi_n(z)\big) \sim C_n \,\mathrm{Ai}\big(\xi_n(z)\big)\,, \tag{2}$$

where $\xi_n(z) = z/z_0 - \lambda_n$ and C_n are normalization constants.

It is useful to give a semiclassical solution of this problem, which is valid with high accuracy ($\sim 1\%$) even for low quantum states. In accordance with the Bohr–Sommerfeld formula, the energies of neutrons in quantum states E_n^{QC} ($n = 1, 2, 3\ldots$) are given by

$$E_n^{\mathrm{QC}} = \left\{\frac{9m}{8}\left[\pi\hbar g\left(n - \frac{1}{4}\right)\right]^2\right\}^{1/3}. \tag{3}$$

The precise energy values E_n (as well as their approximate values E_n^{QC}) depend only on m, g, and $\hbar$, and are independent of the mirror properties. It follows from Eqn (3) that as the quantum state number n increases, the energy of the nth quantum state increases as $E_n^{\mathrm{QC}} \sim n^{2/3}$, while the difference in the energy of neighboring quantum states decreases as $\Delta E_{n+1,n}^{\mathrm{QC}} \sim n^{-1/3}$.

Within the classical description, a neutron with the energy E_n can rise in the gravitational field up to the height $z_n = E_n/(mg)$. In quantum mechanics, the probability of observing a neutron with the energy E_n in the nth quantum state at a height z is equal to the squared modulus of its wave function (2). We can see on left side in Fig. 2 that the squared modulus of the neutron wave function in the nth pure quantum state has n maxima and $n-1$ minima between them; the minimum values and the wave function at zero height are equal to zero, and the wave function tends asymptotically to zero at an infinitely large height. The squared modulus of the neutron wave function is greater than zero at any height $z > 0$; but it is exponentially small at heights z above some critical value z_n corresponding to each nth quantum state; the value of this critical height z_n is equal to the classical turning height for neutrons in this quantum state. The classical turning heights are $z_n = \{13.7, 24.0, 32.4, 39.9\}$ for the four lowest quantum states.

The neutron wave functions $\psi_n(z)$ tend to the following asymptotic functions at large heights $z > z_n$ forbidden in classical mechanics:

$$\psi_n\big(\xi_n(z)\big) \to C_n \xi_n^{-1/4} \exp\left(-\frac{2}{3}\,\xi_n^{3/2}\right). \tag{4}$$

Here, $\xi_n \to \infty$ and C_n are normalization constants.

Using the known eigenfunctions in problem (2), we can calculate their Fourier transform, thus obtaining the amplitudes $\phi_n(v)$ measuring the velocity v of neutrons in the nth quantum state:

$$\phi_n(v) = \sqrt{\frac{m}{2\pi\hbar}} \int_0^\infty \psi_n(z) \exp\left(-\mathrm{i}\,\frac{mvz}{\hbar}\right) \mathrm{d}z\,, \tag{5}$$

where $v_0 = \sqrt{2\varepsilon_0/m} = 1.07$ cm s^{-1} is the characteristic velocity in the problem. The probability $|\phi_n(v)|^2$ of observing neutrons in the nth quantum state as a function of velocity is shown on the right side in Fig. 2 for a few low-lying quantum states.

2.2 Optimum conditions for the observation of gravitational quantum states and the properties of UCNs

We analyze the conditions needed to observe quantum states. A massive object in a sufficiently broad and deep potential well should reside in quantum states, irrespective of the nature of the potential. Examples of such quantum states in electromagnetic and nuclear potentials are well known. Quantum states of electrons in an electromagnetic field determine the structure of atoms, and quantum states of nucleons in a nuclear potential are responsible for the nuclear structure. Analogous quantum states exist in a gravitational field, but they can hardly be observed because of the weakness of the gravitational interaction, and hence because of numerous false systematic effects that usually destroy gravitational quantum states in laboratory conditions. UCNs provide a unique object for such an experiment: their electric charge is zero, and hence competing electromagnetic effects are suppressed; their lifetime is rather long, thus providing the needed high energy resolution in accordance with the energy–time uncertainty relation; the small mass of neutrons favors observation of quantum effects because it allows a large uncertainty of their position in accordance with the position–momentum uncertainty relation; and the neutrons do not reach thermal equilibrium with the mirrors, which allows measurements at ambient temperature (we recall that the UCN energy is lower than the thermal fluctuation energy by many orders of magnitude). Characteristic parameters of the problem allow considering a mirror as an infinitely abrupt and high potential barrier; therefore, the mirror parameters affect neither the energies of neutron eigenstates nor the shape of eigenfunctions.

We list the properties of UCNs that are important for carrying out the presented experiments. The broad attention to applications of UCNs to fundamental particle physics [60–64] is manifested, for instance, in searches for a nonzero electric dipole moment of the neutron [65, 66], in measurements of the free neutron lifetime [62–72], and in verification of the neutron electric neutrality [73]. This is due to a unique property of UCNs, their total reflection from a surface. This property allows long storage of UCNs in closed traps; the storage time may approach the neutron lifetime defined by their β-decay (about 15 min). In other words, the probability of neutron loss in trap walls can be much lower than the

probability of their β-decay. Such long storage of UCN favors precision measurements of neutron properties and their interactions with matter and fields.

UCNs usually reflect from a surface elastically. As a result, thermodynamic equilibrium between neutrons and the mirror (trap) is not reached during the observation time. Similarly, radiowaves do not change their frequency when they reflect from obstacles. This is because the UCN wavelength ($\sim 10^2$ Å) is about 10^2 times larger than interatomic distances in the mirror material. Therefore, UCNs are reflected from a nearly motionless potential resulting from the averaged interaction of UCNs with a huge number of nuclei. We note that the most precise verification of the degree of elasticity of UCN reflection from a surface was obtained in experiments measuring gravitational quantum states of UCNs [74]. The energy of neutron vertical motion in the lowest quantum state in Earth's gravitational field E_1, Eqn (3), corresponds to the temperature ~ 20 nK, which is much smaller than the setup temperature. Nevertheless, the probability of inelastic reflection of UCNs from a surface differs from zero; it is typically equal to $10^{-5}-10^{-4}$ per collision, as shown in [75] and in later publications. The energy of neutrons inelastically reflected from trap walls at the ambient temperature is about the energy of thermal fluctuations, $10^{-2}-10^{-1}$ eV.

Another surprising channel of neutron losses has been observed recently; its probability is $10^{-8}-10^{-3}$ per trap wall collision. It is due to a slight heating [76–81] of UCNs; in this process, the energy increases by only $\sim 10^{-7}$ eV on average, which is much lower than the energy of usual thermal heating, but much higher than the characteristic energy of gravitational quantum states of neutrons. Anyway, inelastic reflection of either kind usually causes a loss of the neutron but not the transition between gravitational quantum states.

In modern UCN sources and designs, the UCNs are an extremely small low-energy fraction of a broader neutron spectrum. The gravitational quantum states of neutrons were observed and studied in a series of experiments carried out using the UCN source of the high-flux reactor at the Institut Laue–Langevin in Grenoble [82].

3. Methods of observation of gravitational quantum states of UCNs

The experimental installation used in the first series of experiments is presented in Section 3.1. It is a one-component gravitational spectrometer of UCNs with a high energy and spatial resolution. The principle of its operation is shown in Fig. 3.

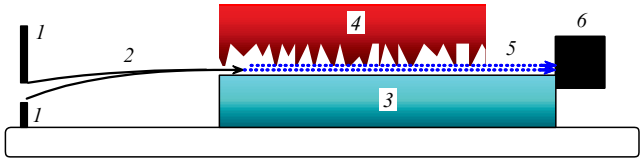

Figure 3. Schematic of the experimental setup in the flow-though mode. *1* are the bottom and top entrance collimator plates, arrows *2* correspond to neutron classical trajectories between the collimator and the entrance to the slit between mirror *3* and scatterer *4*. Dotted horizontal arrows *5* illustrate neutron quantum motion above the mirror. *6* is the neutron detector. The height of the slit between the mirror and the scatterer can be varied and precisely measured.

The experimental method consists in (1) measuring the neutron flux through a slit between the mirror on the bottom and the flat scatterer on top as a function of the slit height (the integral measuring method, Section 3.2), or (2) analyzing the spatial neutron density distribution behind the horizontal bottom mirror exit (the differential measuring method, Section 3.5) using position-sensitive detectors. The slit height can be changed and precisely measured. The scatterer surface is smooth on a large scale but rough on the micrometer scale; the roughness amplitude is about one or a few micrometers, and is comparable to the characteristic scale of the problem z_0. In the classical approximation, the scatterer eliminates neutrons if their vertical velocity component is sufficiently high to raise them up to the scatterer height, but the quantum mechanical description, for instance, must account for the tunneling of neutrons through a gravitational barrier between the classically allowed heights and the scatterer height, which is considered in Section 3.3. Section 3.4 describes the role of the scatterer. Its surface reflects neutrons nonspecularly; therefore, the scatterer mixes the vertical and horizontal velocity components of the neutrons. Because the neutron horizontal velocity components are much larger than their vertical velocity components, such mixing causes numerous collisions between the neutrons and the scatterer, thus causing a prompt loss of these neutrons. The choice of material for the scatterer (or that of the coating on its surface) is not important; the principle cause of neutron loss is neutron scattering on a rough scatterer surface followed by neutron loss in the mirror or in scatterer bulks.

Ideally, the vertical and horizontal motions of a neutron are independent. This statement is valid if neutrons are specularly reflected from the horizontal mirror, and the scatterer or any external forces does not affect the motion of neutrons passing through the slit. In this case, the horizontal motion of neutrons (with the velocity $V_{\rm hor} = 5-10$ m s^{-1}) is governed by classical laws, and vertical motion is quantized; the effective neutron vertical velocity is v_0 (the energy is ε_0).

The length of the bottom mirror is chosen based on the energy–time uncertainty relation, which looks surprising for a setup of macroscopic size. The fact is that observation of quantum states is possible if $\Delta E_{n+1,n} > \delta E_n$ [see Eqn (3)]. As the state number n increases, the energy difference $\Delta E_{n+1,n} \sim n^{-1/3}$ decreases until the levels pass into the classical continuum. Evidently, measurements of low quantum states are easier and more convenient. The quantum state width δE_n is defined by the time of flight of neutrons above the mirror if no quantum transitions between the states occur. Therefore, the mirror length is determined by the time interval needed to observe a neutron in the quantum state ($\Delta\tau \sim \hbar/\Delta E_{n+1,n} \gg 0.5$ m s for low states); it can be about $L \sim 10$ cm for the neutron velocity $V_{\rm hor} = 5-10$ m s^{-1}.

The vertical scale in the problem is defined by the momentum–position uncertainly relation. The fact is that the smaller the neutron vertical velocity component is, the larger the neutron wavelength associated with this velocity component. But the classical height up to which a neutron can rise in the gravitational field cannot be smaller than the quantum mechanical uncertainty of its vertical coordinate, i.e., the neutron wavelength. This relation determines the lowest bound state of neutrons in Earth's gravitational field. The height uncertainty is then $\sim z_0$, and the vertical velocity uncertainty is $\sim v_0$.

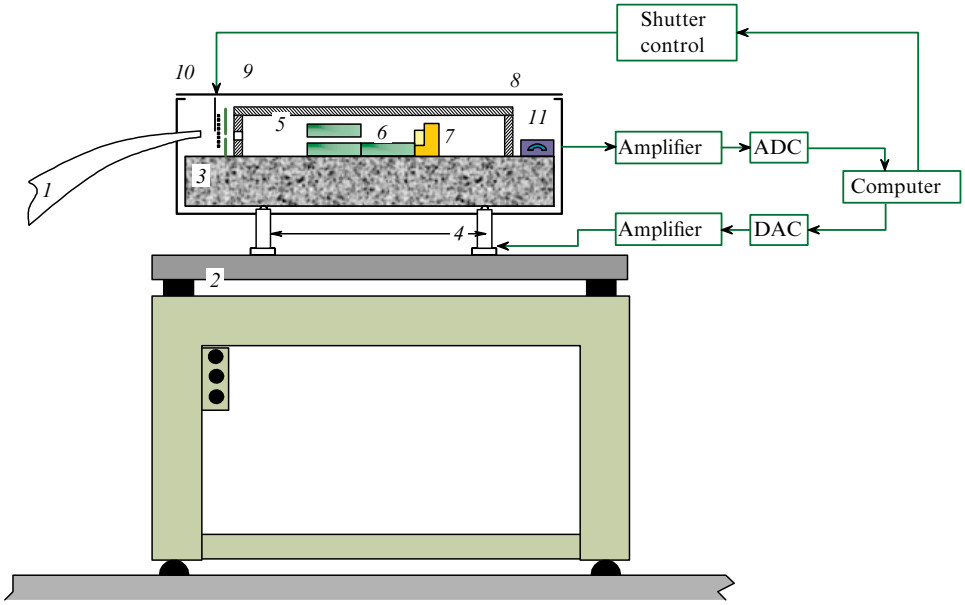

Figure 4. Schematic of the experimental setup used in Ref. [34]: *1* — entrance neutron guide, *2* — passive pneumatic antivibration shielding, *3* — polished granite plate, *4* — piezo-elements, *5* — vacuum chamber, *6* — mirrors and scatterers, *7* — detector, *8* — magnetic screen, *9* — collimator, *10* — neutron valve, *11* — inclinometers, ADC — analog–digital converter, DAC — digital–analog converter.

3.1 Gravitational spectrometer in the flow-through mode

The experimental installation used in the first series of measurements is shown in Fig. 4.

Quantum states are formed above the bottom mirrors. The mirrors and a detector are placed inside a vacuum chamber with an aluminum entrance window of the thickness 30 μm. An adjustable-entrance collimator is installed between the exit of a neutron guide and the entrance to the vacuum chamber; they are separated by the distance about 1.5 cm. The separation between the neutron guide and the experimental setup decouples the setup mechanically from parasitic vibrations of the neutron guide. To prevent parasitic vibrations of the mirrors accompanied by parasitic transitions between the quantum states, the complete setup is mounted on a passive pneumatic antivibration shielding. A set of three interconnected pneumatic valves provides permanent orientation of the 'floating' table relative to the gravitational field direction. A polished granite plate is mounted on the 'floating' optical table using three active piezoelectric legs. The legs are connected in a closed loop with precision inclinometers installed on top of the granite plate. Active adjustment of the length of the piezo-elements provides automatic orientation of the granite plate relative to the direction of the gravitational field with the absolute precision better than 10 μrad. A permalloy magnetic screen protects the vicinity of the mirror against gradients of external magnetic fields. The piezo-elements contribute to changing the positions of optical elements in the installation; capacitors measure positions with an absolute accuracy better than 1 μm. The end piece of the incoming neutron guide is flattened such that it ends with a window 1 cm high and 13 cm wide covered with a thin aluminum window with the thickness 30 μm. Two thick horizontal plates of the entrance collimator are larger in height and width than the window; they absorb neutrons. The height of each plate might be set independently with an accuracy ≈ 10 μm. The entrance collimator, the scatterer, and the bottom mirrors shape the required spectrum of horizontal components of the neutron velocity.

The neutron flux at the entrance to the experimental setup is uniform in height and isotropic in the vertical direction over ranges broader than the angular acceptance of the spectrometer by more than an order of magnitude. The spectrum of neutron velocity horizontal components is shaped using the entrance collimator by setting the two collimator plates to required heights. The background of external thermal neutrons is suppressed by 4π detector shielding. The low-background neutron detector measures the neutron flux at the spectrometer exit. Two ranges of amplitude discrimination of signals from an ^{3}He gaseous detector are set as follows: (1) one range corresponds to a narrow $n + {}^3He \to t + p$-reaction 'peak' $Q = 0.764$ MeV, providing low-background measurements; (2) the other range is much broader ($E > 0.15$ MeV) and allows counting 'all neutron events.' The signal discrimination ranges were typically set such that the electronic efficiency was 50% in the first case and about 90% in the second case. A complex set of collimators and neutron screens protected the detector against scattered ultracold, thermal, and fast neutrons originating from the reactor chamber, as well as from the experimental installation. If the scatterer height is zero and the nuclear reactor is on, the detector count rate is equal, within statistical accuracy, to that measured when the nuclear reactor is off.

3.2 Scanning of neutron density using a scatterer (the integral method)

The method used in the first observation of neutron gravitational quantum states consisted in measuring neutron transmission through a narrow slit Δz between the horizontal mirror and the scatterer above it. In the classical description, the slit size Δz analyzes the neutron velocity vertical components. In the quantum treatment, if $\Delta z \gg z_n$, neutrons in the nth quantum state pass through the slit with no significant loss; but as the slit size decreases, the neutron

wave function $\psi_n(z)$ starts penetrating into the scatterer, and the neutron loss probability increases. If $\Delta z \leqslant z_n$, the slit is practically nontransparent to neutrons in the nth quantum state. In an 'ideal' experiment with an infinitely high energy resolution, the neutron flux $N_{\rm QM}(\Delta z)$ through the slit would sharply change at the height $\Delta z \approx z_n$. For a uniform distribution of neutrons in the phase space, the flux of the neutrons passing through, as a function of the slit height, should tend to the smooth classical dependence at sufficiently large heights Δz:

$$N_{\rm QM}(\Delta z) \to N_{\rm cl}(\Delta z) \sim (\Delta z)^{3/2}\,. \tag{6}$$

Expression (6) is valid if the scatterer efficiency is equal to unity in the classical approximation. A comparison of experimental data with asymptotic dependence (6) provides a good quality test for the scatterer. If the dependence $N(\Delta z)$ is weaker than $\sim (\Delta z)^{3/2}$ as a function of the slit height Δz, then the scatterer efficiency is low.

If a mirror is installed on top instead of the scatterer, then the flux of neutrons passing through the slit must behave linearly,

$$N_{\rm test}(\Delta z) \sim \Delta z\,, \tag{7}$$

as a function of the slit height. This assumption might be verified. It corresponds to the limit of a 'very bad' scatterer.

In an experiment with a mirror on the bottom and a scatterer on the top, the flux of neutrons $N(\Delta z)$ passing through the slit should be suppressed compared to the flux $N_{\rm cl}(\Delta z)$ calculated in the classical approximation. The strongest suppression is expected if $\Delta z < z_1$. Neglecting the stepwise character of the flux of neutrons passing through the slit for heights $\Delta z > z_1$ ('fine structure'), we can write the 'zeroth' approximation

$$N_{{\rm QM},0}(\Delta z) \sim (\Delta z - z_1)^{3/2}\,, \tag{8}$$

where the shift $z_1 \approx 15$ μm in the dependence $N_{{\rm QM},0}(\Delta z)$ corresponds to the lowest quantum state energy $E_1 \approx 1.41$ peV, or, in other words, to the effective decrease in the phase space volume available for neutrons compared to that in the classical model; this shift is due to the uncertainty relation. The 'zeroth' approximation describes the data quite well because the idealized step-like dependence is smoothened due to two factors: the spectrometer experimental resolution and the smooth shape of neutron wave functions; the latter is due to the tunneling of neutrons through the gravitational barrier separating the classically allowed heights and the scatterer height. This phenomenon is considered in Section 3.3.

3.3 Tunneling of neutrons through a gravitational barrier

The first theoretical model for the interaction of neutrons in gravitational quantum states with a scatterer takes the key effect into account: tunneling of neutrons through a gravitational barrier separating classically allowed heights and the scatterer height [29, 45]. This model can be presented in simple analytic expressions. We consider this model in detail in this section, and briefly present new options provided by other models [46–48] in Section 3.4.

We analyze the neutron wave function shapes shown in Fig. 2. For classically forbidden heights $z > z_n$, the asymptotic expressions for the wave functions $\psi_n(z)$ are given by (4). Such a penetration of neutrons to classically forbidden heights is a purely quantum phenomenon called the tunneling effect. It is precisely this phenomenon that defines the spectrometer spatial resolution in the integral measuring mode, because the gravitational barrier penetrability does not change sharply enough as a function of the scatterer height. We follow the standard method of describing nuclear α-activity in the framework of the Gamow theory. The lifetime of an α-active nucleus is equal to the nuclear potential barrier penetrability for an α-particle times the frequency of collisions of an α-particle with this barrier. To estimate the neutron lifetime in our case, we assume that the neutron loss per unit time is proportional to the probability of observing a neutron at the scatterer height. The unperturbed density probability $|\psi_n(\xi(z))|^2$ of observing a neutron at the height z in the classically forbidden range $z > z_n$ is equal to the squared modulus of the neutron wave function in (4):

$$\left|\psi_n\left(\xi_n(z)\right)\right|^2 \to C_n^2\,\xi_n^{-1/2} \exp\left(-\frac{4}{3}\,\xi_n^{3/2}\right), \qquad \xi_n \to \infty\,. \tag{9}$$

In fact, the neutron wave function inside the scatterer is different from the nonperturbed wave function given by (4). Neglecting this perturbation and any factors depending smoothly on ξ, we can estimate the probability $P_n^{\rm tunnel}(\Delta z)$ of observing a neutron in the nth quantum state inside the scatterer at the height $\Delta z > z_n$ as

$$P_n^{\rm tunnel}(\Delta z) = \int_{\Delta z}^{\infty} \left|\psi_n(z)\right|^2 {\rm d}z \approx \exp\left(-\frac{4}{3}\,\xi_n^{3/2}\right), \tag{10}$$

where $(\Delta z - z_n)/z_0$, $\Delta z > z_n$. This expression can also be obtained in calculations of the probability of neutron tunneling through a gravitational barrier in the semiclassical approximation. As is clear from (10), the probability $P_n^{\rm tunnel}(\Delta z)$ decreases sharply as Δz increases if $\Delta z > z_n$. If the scatterer height is smaller than the classical turning height for a neutron in the nth quantum state ($\Delta z < z_n$), then the probability $P_n^{\rm tunnel}(\Delta z)$ is high; it can then be approximated by unity:

$$P_n^{\rm tunnel}(\Delta z) = 1\,, \qquad \Delta z \leqslant z_n\,. \tag{11}$$

Because of the neutron tunneling through the gravitational barrier to the scatterer, the quantum states are quasi-stationary. The neutron loss probability, or the reciprocal neutron lifetime in the nth quantum state $(\tau_n^{\rm abs}(\Delta z))^{-1}$, can be estimated as the frequency ω_n of their 'collisions' with gravitational barrier times the probability of their tunneling to the scatterer:

$$\frac{1}{\tau_n^{\rm abs}(\xi_n(\Delta z))} \approx \begin{cases} \omega_n \exp\left(-\dfrac{4}{3}\,\xi_n^{3/2}\right), & \xi_n > 0\,, \\ \omega_n\,, & \xi_n \leqslant 0\,, \end{cases} \tag{12}$$

$$\omega_n = \frac{\Delta E_{n+1,n}}{\hbar} \approx \sqrt[3]{\frac{m\pi^2 g^2}{3\hbar(n-1/4)}}\,. \tag{13}$$

We consider the passage of neutrons with the horizontal velocity component $V_{\rm hor}$ in the direction along the neutron beam axis through a slit with height Δz between the mirror and the scatterer. During the neutron passage through the slit of length L, $\tau^{\rm pass}(V_{\rm hor}) = L/V_{\rm hor}$, the nth quantum state partly decays. The probability of neutron passage through

the slit is then

$$P_n(\Delta z, V_{\rm hor}) = \exp\left(-\frac{\tau^{\rm pass}(V_{\rm hor})}{\tau_n^{\rm abs}(\Delta z)}\right). \qquad (14)$$

If the scatterer height is small, $\Delta z < z_n$, then the neutron lifetime $\tau_n^{\rm abs}(\Delta z)$ in the nth quantum state is much smaller than the time $\tau^{\rm pass}(V_{\rm hor})$ of neutron passage through the slit between the mirror and the scatterer. Therefore, the probability $P_n(\Delta z, V_{\rm hor})$ in (14) is small; hence, a precise expression for tunneling probability (11) is irrelevant. Finally, the flux of neutrons passing through in several quantum states can be written as

$$F(\Delta z, V_{\rm hor}) = \sum_n F_n(\Delta z, V_{\rm hor}) = F_0 \sum_n \left(\beta_n \exp\left(-\frac{L}{V_{\rm hor}}\sqrt[3]{\frac{m\pi^2 g^2}{3\hbar(n-1/4)}}\right) \times \begin{cases} \exp\left[-\frac{4}{3}\left(\frac{\Delta z - z_n}{z_0}\right)^{3/2}\right], & \Delta z > z_n \\ 1, & \Delta z \leqslant z_n \end{cases}\right), \qquad (15)$$

where β_n is the population in the nth quantum state and F_0 is a normalization constant. The sharpness of the dependence $F_n(\Delta z, V_{\rm hor})$ in (15) on the parameter Δz in the range $\Delta z > z_n$ defines the accuracy with which neutron quantum states can be resolved in measuring the total flux of neutrons passing through the slit; therefore, the sharpness of this dependence defines the best achievable spatial resolution of our spectrometer.

The dependence of the quantum state lifetime on the parameter Δz is the sharper, the larger the difference $\Delta z - z_n$, although the spectrometer spatial resolution increases logarithmically slowly as the quantum state lifetime increases. Better spatial (energy) spectrometer resolution corresponds to a longer time of neutron observation in a quantum state in the slit between the mirror and the scatterer, i.e., to a longer length L of the mirror–scatterer pair or to a smaller velocity $V_{\rm hor}$. The energy resolution is calculated as a function of the observation time, e.g., in Ref. [46]. But the freedom to significantly decrease $V_{\rm hor}$ or to increase L is limited by technological constraints. This means [34] that the spectrometer resolution is determined essentially by a fundamental physics phenomenon, the neutron quantum tunneling through a gravitational potential barrier. The spatial spectrometer resolution can be significantly improved only if the neutron lifetime in quantum states increases by several orders of magnitude using the quantum trap of the GRANIT (GRAvitational Induced Neutron Transitions) spectrometer [43]. Another method of significantly improving the spectrometer resolution is based on using precision position-sensitive neutron detectors [34], to be described in Section 3.5, or by measuring the frequency of resonant transitions or interference between quantum states.

The model expression in (15) is calculated for low quantum states neglecting the perturbation of the neutron wave functions by the scatterer. In fact, the scatterer 'pushed out' the wave functions. Therefore, the values z_n obtained from approximate expression (15) are systematically slightly smaller than the corresponding nonperturbed values. Moreover, we use approximate asymptotic expressions for neutron wave functions; this expression must be corrected if $\xi_n < 1$. Nevertheless, expression (15) provides a good description of the principle physics phenomena concerned; it can be used for approximate data analysis in the form

$$F(\Delta z, V_{\rm hor}) = \sum_n F_n(\Delta z, V_{\rm hor}) = F_0 \sum_n \left(\beta_n \exp\left(-\alpha\frac{L}{V_{\rm hor}}\sqrt[3]{\frac{m\pi^2 g^2}{3\hbar(n-1/4)}}\right) \times \begin{cases} \exp\left[-\frac{4}{3}\left(\frac{\Delta z - z_n}{z_0}\right)^{3/2}\right], & \Delta z > z_n \\ 1, & \Delta z \leqslant z_n \end{cases}\right), \qquad (16)$$

where α is a constant accounting for the finite scatterer efficiency. This formula describes the experimental data using a minimum number of free parameters. The effective 'height' of a rough scatterer is defined in the first approximation as the mean-weighted height averaged over a surface if the roughness amplitude is significantly smaller than z_0. If the roughness amplitude is larger than or comparable to the problem characteristic scale z_0, then the definition of the scatterer height should be reconsidered using more general models. However, as shown in Section 4, the presented model is quite precise for the analysis of the measured experimental data.

3.4 Models describing the interaction of neutrons in quantum states with a scatterer

The model in [48] results in analytic expressions for the flux of neutrons passing through a slit between a mirror and a scatterer that are similar to those in (16). The difference consists in replacing the integration limits in (10); these limits affect the probability of neutron loss per semiclassical collision with the scatterer. In the model in [45], the neutron loss probability is proportional to the squared amplitude of the nonperturbed neutron wave function in the corresponding quantum state, and the scatterer efficiency is proportional to the squared amplitude of scatterer roughness times a free parameter. The model in [48] takes the deformation of neutron wave functions caused by the scatterer into account. The model assumes that the wave function vanishes on the scatterer surface (the dominant contribution to the wave function deformation), and the probability loss is proportional to the integral of the overlap of the squared nonperturbed neutron wave function and the range of scatterer roughness. In the limit of a large scatterer roughness amplitude, the model in [48] reduces to that in [45] with a rescaled normalization constant.

But the model in [48] allows analyzing experiments not only in the standard geometry shown in Fig. 3 but also in the so-called reversed geometry, with a scatterer on the bottom and a mirror on the top. Such measurement is very sensitive to the scatterer quality; it also provides a sensitive test of the correctness of the theoretical description. Figure 5 taken from [48] illustrates the precision of the model description of the experimental data in two geometries simultaneously using equal free parameters.

A 'first-principle' theoretical description of the interaction of UCNs in quantum states with a scatterer is presented in Refs [46, 47] for roughness of a small amplitude and a short correlation length; there are no free parameters involved: the choice of scatterer parameters corresponded to the performed experiments. The rough scatterer surface was regarded as a time-dependent boundary condition in the reference frame of a moving neutron. This problem, in turn, reduces to the one

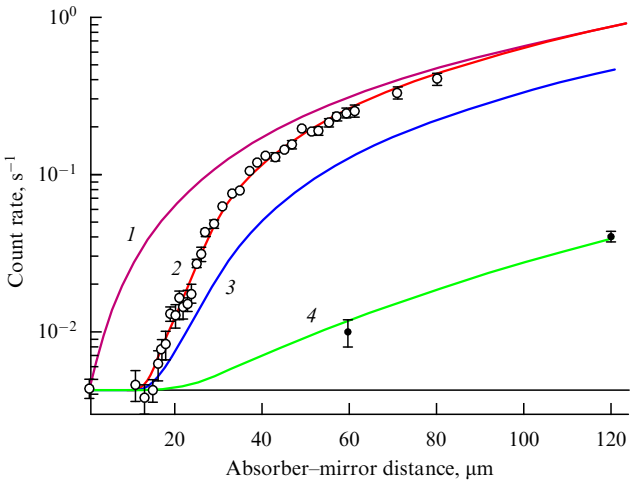

Figure 5. Empty circles correspond to the measured flux of neutrons passing through the horizontal slit between the mirror and the scatterer as a function of the scatterer height. Black circles indicate the data measured 'in reverse geometry,' i.e., with the scatterer above and the mirror below. Line *1* corresponds to the classical model in standard geometry; line *2* provides the results of approximating the data measured in standard geometry using the theoretical model in [48]; gravity is taken into account; line *3* indicates an analogous curve calculated for zero gravity (it coincides with that calculated for the reverse geometry); line *4* shows the results of approximating the data measured in the reverse geometry using the theoretical model in [48]; the parameters of the model are equivalent to those used in the standard geometry. The horizontal line indicates the detector background.

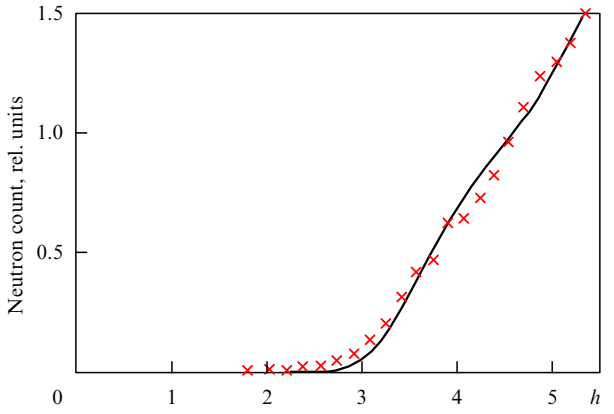

Figure 6. The flux of neutrons through the slit between the mirror and the scatterer is shown as a function of the slit height h (in units of the characteristic height z_0). The solid line indicates the results of theoretical calculation 'from first principles' [47]; crosses show the experimental results [29]. The scatterer roughness amplitude is 0.7 μm, the correlation length is 7 μm, and the quantum state populations are equal.

with a time-dependent perturbation potential. It can be solved exactly and provides the probabilities of quantum transitions between quantum states in the system, including the mirror, the scatterer, and the gravitational field. Moreover, the exact solution for the dynamics of quantum state populations is obtained. It describes the measured data well (Fig. 6). We note that neither the quantum state populations (which are assumed to be equal) nor the characteristic quantum state heights z_n are free parameters in this model.

The most difficult case for all the presented models is the limit of large roughness amplitudes (compared to z_0), because the scatterer height is poorly ill-defined in this limit case. But this case is interesting from the methodological standpoint, because it provides a maximum scatterer efficiency. The limit of large roughness amplitudes will be explored using the GRANIT spectrometer described in Section 5.3.

3.5 Measurement of the neutron density above a mirror using position-sensitive detectors (the differential method)

To resolve excited quantum states and to precisely measure their parameters, other methods can also be used, for instance, the so-called differential method [40] using position-sensitive detectors with a very high spatial resolution (~ 1 μm), developed for this particular task [34]. The differential method also allows directly measuring the distribution of neutron density under a gravitational barrier, or, in other words, the neutron tunneling through the gravitational barrier.

Direct measurement of the spatial density distribution in the standing neutron wave above the mirror is preferable to its scanning using a scatterer at a variable height. The differential method allows measuring the probability of observing neutrons at all heights of interest simultaneously, while the information on the probability of observing neutrons at some height is obtained by integral methods by subtracting the neutron flux values measured with the scatterer lifted to two close heights. It is clear that the differential method is much more sensitive than the integral one; it therefore provides the required statistical accuracy for much shorter times. This last advantage is important because of the extremely low count rate in such an experiment, even when the largest UCN fluxes currently available are used. Moreover, the scatterer used in the integral method unavoidably disturbs the measured quantum states: it deforms the wave functions and shifts the energy eigenvalues. The finite accuracy of calculating these deformations causes systematic uncertainties, which limit the ultimate accuracy of measurements of the quantum state parameters. For this and other reasons, the use of position-sensitive detectors is very attractive for direct measurements of the spatial distribution of observing neutrons above a mirror. But detectors with a spatial resolution ~ 1 μm had not existed before the experiments presented here were performed. That is why we had to propose and develop detectors of such a type, as well as methods of their treatment. This resulted in plastic position-sensitive nuclear track detectors (CR39) with a thin uranium ($^{235}UF_4$) or boron (^{10}B) coating, as described in Ref. [34] (Fig. 7).

Tracks are produced in plastic by daughter nuclei emitted in the neutron-induced fission of ^{235}U nuclei. Then they are increased in diameter to ≈ 1 μm through chemical etching in an alkali solution. After being developed, such a detector with the size of several centimeters is scanned using an optical microscope with the positioning accuracy ≈ 1 μm. The sensitive ^{235}U layer is thin enough (thinner than 1 μm) for the points of entry of daughter nuclei into the plastic to nearly coincide with the points of neutron entrance into the uranium layer. On the other hand, the sensitive layer is thick enough to provide significant UCN detection efficiency (about 30%). The measuring method and data analysis are presented in Ref. [31].

We also studied analogous detectors with a boron coating. The efficiency of such detectors for UCNs can be higher (due to a significantly larger cross section of their interaction with neutrons). On the other hand, there are inherent larger backgrounds because of difficulties related to identification of relatively short tracks of the α-particle induced by

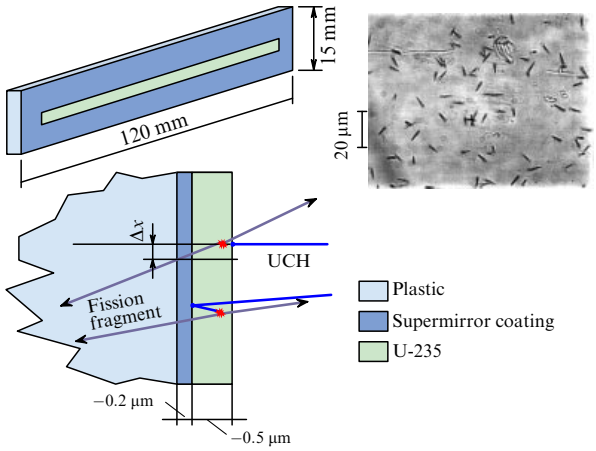

Figure 7. Position-sensitive plastic nuclear-track neutron detectors (CR39) with a thin uranium coating ($^{235}UF_4$). The size of the sensitive uranium layer in the detector is 5×100 mm, and the size of the plastic plate is 15×120 mm. The characteristic thickness of the uranium layer is 0.5 μm. The inset on the right shows the detector surface after chemical etching measured using a scanning optical microscope.

neutrons. Alternative types of position-sensitive real-time detectors are developed in Refs [83, 84]. Although the spatial resolution of such detectors (about 5 μm) is still not high enough for directly measuring the neutron wave functions in gravitational quantum states, the option itself of real-time measuring is very attractive.

Measurements with position-sensitive detectors were analyzed in Ref. [40], aiming at their optimization for identification of neutron quantum states. The spatial neutron density variation above the mirror is poorly pronounced for a large number of equally populated states. But the contrast can be increased significantly if quantum states are populated properly. The fact is that each squared modulus of the neutron wave function $|\psi_n(z)|^2$ in a quantum state n (corresponding to the probability of observing a neutron at the height z above the mirror surface) has n maxima and $n-1$ minima, equal to zero, between them (see Fig. 2), as it is for any standing wave. The height ~ 10 μm of the first maximum of $|\psi_1(z)|^2$ is approximately equal to the lowest first minima of $|\psi_n(z)|^2$ for several low quantum states, other than the lowest state. An ideal experiment would consist in separating one or a few quantum states with $n > 1$ and then measuring the probability of observing a neutron as a function of the height above the mirror using a position-sensitive detector with a spatial resolution ~ 1 μm. Thus, a few low quantum states ($n > 1$) contribute 'coherently': the probability of observing a neutron at a height ~ 10 μm is much smaller systematically than the probability of observing a neutron at other close heights.

We consider a scheme of such an experiment. One or two low quantum states can be separated using the standard scatterer method [28]; the energy spectrometer resolution is high enough for this purpose. The method of neutron nonresonant transition from low quantum states to higher ones [40] involves using a mirror on the bottom with a small negative step. Neutrons reside in quantum states on the left and the right of the step. But the neutron wave functions in quantum states with an equal quantum number on the left and right of the step are shifted relative to each other by the step height Δz_{step}. Neutrons in the nth quantum state $\psi_{n,\,\text{before}}(z) = \psi_n(z + \Delta z_{\text{step}})$ on the left of the step populate quantum states $\psi_{n,\,\text{after}}(z) = \psi_n(z)$ after the transition through the step, with probabilities equal to $\beta_{nk}^2(\Delta z_{\text{step}})$. In this case, the step can be considered an infinitely fast perturbation; the transition matrix elements $\beta_{nk}(\Delta z_{\text{step}})$ can then be written as

$$\beta_{nk}(\Delta z_{\text{step}}) = \int_0^\infty \psi_n(z + \Delta z_{\text{step}})\,\psi_k(z)\,\mathrm{d}z\,. \tag{17}$$

If the negative step is high enough, for instance, if its height is equal to 15 μm, then the probability β_{n1}^2 of observing a neutron in the lowest quantum state after transition through the step is extremely small. This is because the spatial size of the neutron wave function in the lowest quantum state $\psi_1(z)$ after transition through the step is smaller than 15 μm.

The results of measurements of the state prepared in such a way is given in Section 4.3.

4. Observation and study of neutron gravitational quantum states

Neutron gravitational quantum states were studied in the gravitational spectrometer described in Section 3.1 using the integral flow-through method (see Section 3.2). In a first series of experiments (Section 4.1), the lowest quantum state was reliably identified, and any major systematic false effects were eliminated. In a second series of experiments (Section 4.2), the parameters of the two lowest quantum states were measured, and any eventual systematic effects were studied in detail. The feasibility of using the differential flow-through method (Section 3.5) was investigated experimentally (Section 4.3). The measured experimental data were analyzed using the models considered in Section 3.3.

4.1 Observation of the lowest quantum state

The first measurement [27, 28] was aimed at the experimental observation of neutron gravitational quantum states using the integral method. Particular attention was given to observing the most characteristic property of such a system, the nontransparency of the slit between the mirror and the scatterer to neutrons if the slit height does not exceed the characteristic spatial size of the lowest quantum state $\Delta z < z_1$. We also studied and eliminated eventual systematic effects.

Neutrons with a broad distribution of initial velocities, coordinates, and angles arrive at the experimental setup entrance. The spectrum of the horizontal components of the neutron velocity is measured using horizontal plates in the entrance collimator with adjustable heights. Figure 8 illustrates a scheme of the integral method of measuring this spectrum. Neutrons passing through the slit between the mirror and scatterer move in zone l along parabolic trajectories that are lower than the scatterer height but higher than the bottom mirror height. This condition and the smallness of the scatterer/mirror slit size (compared to the entrance collimator slit size) uniquely relate the value V_{hor} to the difference Δl between the neutron turning point height and its trajectory height in the entrance collimator. The time of flight τ_l between the collimator and the mirror is $\tau_l = l/V_{\text{hor}}$; the difference between the neutron turning height and the neutron trajectory height in the entrance collimator is $\Delta l = g\tau_l^2/2$; the neutron horizontal velocity

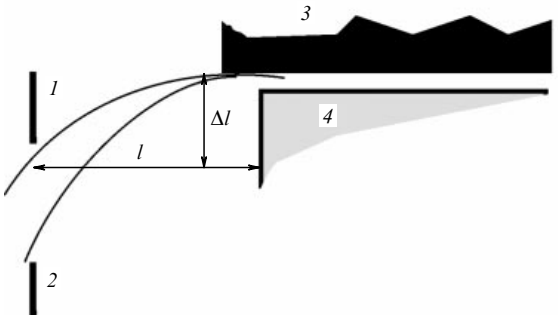

Figure 8. A scheme for measuring and shaping the spectrum of horizontal velocity components $V_{\rm hor}$: *1* and *2* — the entrance collimator plates; each plate could be set to the required height independently; *3* — scatterer; *4* — mirror; *l* is the distance between the entrance collimator and the mirror. Neutron trajectories rise to the height Δl along this path, and become horizontal at the entrance to the slit between the mirror and the scatterer.

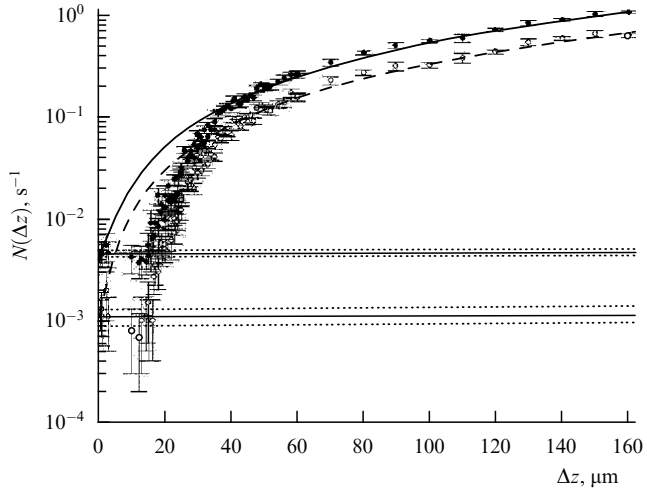

Figure 9. A typical flux $N(\Delta z)$ of neutrons passing through the slit between the mirror and the scatterer is shown as a function of the slit height Δz; the two mirrors on the bottom with the length 6 cm each are installed such that their surfaces are parallel to each other. Black circles indicate the data measured with the differential range of discrimination of the detector signal amplitude corresponding to counting 'all neutron events.' The solid line approximates the data using the classical dependence $N_{\rm cl}(\Delta z)$. Open circles show the data measured with the differential range of discrimination of the detector signal amplitude corresponding to a narrow peak in the reaction $n + {}^3He \to t + p$. The dashed line is an approximation of these data by the classical dependence $N_{\rm cl}(\Delta z)$. The horizontal lines show the detector background values and their uncertainties measured with the reactor turned off.

component along the neutron beam can therefore be calculated as $V_{\rm hor} = l\sqrt{g/(2\Delta l)}$.

The vertical angular divergence ($\approx 4 \times 10^{-2}$) is fixed using the titanium collimation plate height and the bottom mirror front edge position. The scatterer–mirror system decreases the range of neutron vertical velocity components by an order of magnitude. Neutron transmission through the slit between the mirror and the scatterer was measured as a function of the setup inclination angle. This measurement showed no angular dependence, thus proving a uniform distribution of neutrons in the initial phase space. The upper cut-off for the vertical velocity components is defined using the scatterer height above the mirror. Only neutrons arriving at the front mirror edge with a small vertical velocity component can pass through the slit. This condition also allows selecting a range of velocities $V_{\rm hor}$. The lower cut-off for the velocity components $V_{\rm hor}$ is determined by a parabolic trajectory starting just above the edge of the bottom collimation plate. The upper cut-off is determined by a parabolic trajectory starting just below the edge of the top collimation plate.

The phase space volume corresponding to a single quantum state is small. For example, the neutron flux in the 'quantum mode' (low scatterer) (Fig. 9) was $10^{-3} - 10^{-1}$ s^{-1}, while the total neutron flux through the entrance neutron guide was 10^6 s^{-1}, i.e., larger by a factor of $10^7 - 10^9$. Therefore, efficient suppression of backgrounds is important. The background of external thermal neutrons was suppressed with 4π boron rubber B_4C shielding. A long narrow channel in the shielding with a height of only a few millimeters allows passing neutrons along parabolic trajectories to the entrance to the slit between the mirror(s) on the bottom and the scatterer on the top, and then their passing through the slit to the detector. Particular attention was paid to the contribution to neutron background that could originate from multiple elastic reflection of UCNs inside the experimental setup. Multi-slit shielding between the entrance aluminum window and the mirrors protects the detector against the UCNs up-scattered to the thermal energy range in the neutron guide, at the entrance to the setup and in the collimator itself. However, this shielding does not affect the spectra of vertical and horizontal velocity components of counted neutrons. Neutrons settled in quantum states were moving along parabolic trajectories in front of the slit between the mirror and scatterer. The upper titanium plate in the entrance collimator closes the direct view to the detector.

Mirrors on the bottom are polished plates of optical glass. The bottom mirror surfaces were examined using small-angle X-ray scattering. The mean-square roughness amplitude was 1–2 nm, and the correlation length was ≈ 10 μm. Scatterers are macroscopically flat glass plates with high roughness. The roughness amplitude is about 1 μm, while the correlation length is a few micrometers. One plate is coated with a Ti–Zr–Gd alloy (in the ratio 54 : 11 : 35, with the thickness 0.2 μm; such a coating is typically used as an antireflecting sublayer in cold neutron polarizers [85, 86]) using magnetron sputtering. Neutrons could be absorbed in this layer or scattered nonspecularly. Nonspecular reflection 'mixes' horizontal and vertical neutron velocity components, thus sharply increasing the rate of neutron collisions with the scatterer. This process eliminates neutrons with large vertical velocity components. The classical estimation of the distance $\Delta l_{\rm cl}$ between two consequent collisions of neutrons with the bottom mirror (assuming that the neutrons do not touch the scatterer) is $\Delta l_{\rm cl} = 2V_{\rm hor}\sqrt{2H_0/g}$.

For the neutron spectra and slit sizes used, neutrons cannot pass through the slit (in the classical approximation) without touching the bottom mirror and/or the scatterer if the mirror and scatterer are longer than 10 cm. This condition allows estimating the minimum mirror length that is sufficient for shaping the vertical velocity component spectrum. The uncertainty relation provides an even smaller value for the minimum mirror length needed for resolving the quantum states: $\Delta l_{\rm QM} = V_{\rm hor}\hbar/\Delta E_{1,2}$ (for the two lowest quantum states). In fact, the mirror length should be much larger than these minimum estimates.

We measured the transmission of neutrons through the slit between the mirror on the bottom and the scatterer on the top as a function of the scatterer height. The scatterer was installed on three active piezo-elements. The length of each such leg could be adjusted within the range of 25 μm. A set of precision two-axis inclinometers measured relative scatterer translation when one piezo-element shortened or elongated. A cylindrical gaseous ^{3}He detector (2.3 bar Ar, 30 Torr ^{3}He, 10 Torr CO_2, length ≈ 20 cm, diameter ≈ 1.7 cm) measured the neutron flux $N(z)$. An entrance window with the length 12 cm and height 1.5 mm is made of aluminum foil with the thickness 100 μm. The detector is placed inside the vacuum chamber; it operates without discharges only if the residual gas pressure is lower than $\approx 2 \times 10^{-2}$ Torr. The aluminum entrance window would reflect neutrons with the longitudinal velocity component smaller than 3.2 m s^{-1}, but aluminum windows (*1*, Fig. 4) at the neutron guide exit, as well as the windows at the entrance to the vacuum chamber (*5*, Fig. 4), have already reflected such neutrons. With the nuclear reactor off and on, the background was respectively equal to $(1.3 \pm 0.2) \times 10^{-3}$ s^{-1} and $(4.6 \pm 0.3) \times 10^{-3}$ s^{-1}. As is clear from Fig. 9, the background was efficiently suppressed: with zero scatterer height and the nuclear reactor on, the detector count rate was equal to that measured with the nuclear reactor off within statistical accuracy. Other background sources, such as thermal neutrons in the reactor hall or UCNs scattered elastically or inelastically inside the experimental setup, were negligible.

Two principle configurations of mirrors and scatterer were used. The width of the two identical bottom mirrors in the first experiment was 10 cm, and the length was 6 cm. Both mirrors were installed one behind the other, with the horizontal slit between them smaller than 5 μm. The heights of the mirrors were equal, with an accuracy of at least a few micrometers. The scatterer width was 10 cm, and its length was 13 cm. The scatterer overhung from the mirror towards the entrance such that it did not cover 2 cm of the second mirror on its exit side. In the second experiment, one bottom mirror with the same height and width and with the length 10 cm replaced the two bottom mirrors used in the first experiment.

A comparison of the experimental data with a known asymptotic curve is a good test of the scatterer quality. Figure 9 illustrates that the classical model $N_{\rm cl}(\Delta z)$ approximates the experimental data well when the scatterer height Δz is large. On the other hand, if another mirror is installed on the top instead of the scatterer, we should obtain expression (7). In fact, this dependence was confirmed in measurements with two mirrors. The expected quantum mechanical dependence $N^0_{\rm QM}(\Delta z)$ also approximates the general behavior of the experimental data for small scatterer heights. The results of the rigorous quantum mechanical treatment in Refs [45–48] do not differ within the uncertainties of the first experiment from those obtained within the mentioned simplified description; the rigorous description provides smoother dependences. The data do not confirm the classical dependence $N_{\rm cl}(\Delta z)$, in particular, if $\Delta z < 20$ μm; but they agree with the quantum mechanical models $N^0_{\rm QM}(\Delta z)$ and $N_{\rm QM}(\Delta z)$. Neutron fluxes are independent of the neutron horizontal velocity component or of the neutron wavelength within experimental uncertainties. Only the vertical component of the neutron velocity is relevant.

The scatterer efficiency was also measured. For this, the scatterer was installed on the bottom and a mirror 10 cm long was placed on top (reverse geometry). Such an assembly must be nontransparent to neutrons if the scatterer efficiency is 100%. A small neutron flux through the slit allows estimating the finite scatterer efficiency. The efficiency appeared to be higher than 95% for the slit size 120 μm and higher than 98% for the slit size 60 μm. A semiclassical estimation of the distance between two consecutive collisions with the scatterer surface yields the mean scatterer efficiency higher than 90% per bounce. Therefore, the scatterer efficiency is by far sufficient for excluding eventual false effects in the main experiment. The ratio of the neutron flux in the standard geometry (scatterer on the top) to the neutron flux in the reverse geometry (scatterer on the bottom) is about 20 if the slit size is 120 μm; this ratio is nearly 50 if the slit size is 60 μm. These differences are due to the gravitational field. With zero gravity, these measurements (in standard and reverse geometries) would provide equivalent results.

We analyze the reliability of the experimental results and consider systematic uncertainties that could affect the interpretation of the data concerning the fact of observation of the lowest neutron gravitational quantum state. The beam-related background is negligible if the scatterer height is smaller than ≈ 15 μm (see Fig. 9). The experimental data are quite reproducible: the 'nontransparency' of the slit between the mirror and the scatterer for small slit sizes was measured 11 times with various configurations of mirrors. The precision of mirror, scatterer, and collimator production is high enough to exclude any problems related to their shape. X-ray studies of the mirror surfaces confirmed that the probability of nonspecular reflection of neutrons was at least smaller than 1%. This is an important point because a situation can be imagined where the neutron transmission through the slit is suppressed because of the low quality of the bottom mirror. The quantity of neutron reflections from the bottom mirror can be estimated in the classical approximation, and the factor of suppression of the neutron flux for small scatterer heights can be calculated using the experimental data. Then the observed neutron flux suppression through the slit, when the slit size is small, can be explained by the low quality of the mirror only if the probability of nonspecular reflection reaches $\sim 60\%$, which evidently contradicts the data measured using X-rays. Besides, the neutron transmission would then depend on the horizontal neutron velocity component; this hypothesis also contradicts the data.

The experimental setup was surrounded with a permalloy screen; residual magnetic field gradients (which would result in an effective 'curvature' of the mirror surface) were negligible. To avoid parasitic suppression of neutron transmission through the slit between the mirror and the scatterer, caused by neutron diffraction on the entrance angle of the bottom mirror, the angular divergence in the initial neutron beam was shaped broadly enough. The diffraction angle for neutrons in the lowest quantum state was much smaller than the angular spread in the initial neutron beam. Moreover, the diffraction effect would strongly depend on the neutron wavelength defined by the horizontal neutron velocity component. This hypothesis contradicts the data.

A false effect caused by a systematic shift of the zero scatterer height is excluded. The maximum resulting uncertainty in measuring the scatterer height was a few micrometers if the slit size was smaller than 100 μm. This uncertainty is not necessarily negligible for medium and large scatterer heights due to the accumulation of uncertainties after many consecutive height settings, and due to the

poor control of the slow drifting of the legs or inclinometer electronics. However, the results presented in this section are clearly free of noticeable systematic errors in measuring small scatterer heights.

In later experiments, the scatterer height was measured using the absolute capacitance method. Many additional tests of reliability of the scatterer height measurements were also carried out. For instance, the height was monitored using precision mechanical devices (comparators) with the accuracy ≈ 1 μm. The scatterer was raised and descended to a zero height. Such translation could be easily monitored using inclinometers as the scatterer touched the bottom mirror in this case. The repeatability and stability of the neutron count rate were permanently monitored as well. In some measurements, the system of piezo-elements was replaced by foil spacers of a known thickness placed between the mirror and the scatterer. Each test provided a positioning precision of at least a few micrometers when the scatterer height was small. Observation of the transparency of a 15 μm slit between the mirror and the scatterer for visible light also proved the absence of significant shifts in measuring the scatterer height. We note that the neutron flux through such a slit was zero (see Fig. 9).

Based on all the arguments presented above, we can conclude that the slit between the mirror and the scatterer is not transparent to neutrons when the slit height is smaller than 15 μm, due to quantization of neutron states in the gravitational field above the mirror. The lowest neutron quantum state in Earth's gravitational field was observed for the first time in the measurement described here.

The experimental task of observing higher quantum states is more challenging than measurements of the lowest quantum state: to observe the neutron flux populating the lowest quantum state, we have to compare the nearly zero count rate in the detector (if the background is low) with a significantly larger count rate, while for resolving higher quantum states, we have to compare two nonzero neutron fluxes of close intensity. Moreover, the first step in the neutron flux as a function of the scatterer height is the largest; the step size decreases rapidly as the quantum number increases. Therefore, even for an equal experimental resolution of each step, their separation becomes more difficult for higher quantum states. In addition, both the difference in energy between neighboring quantum states and the experimental accuracy decrease as the quantum number increases. Difficulties in observing higher quantum states can be divided into two groups. The first concerns the experimental setup quality (for instance, precision in setting the scatterer height and properties of the neutron beam); these problems can be overcome in principle. The second group deals with constraints imposed by quantum mechanics (elimination of neutrons in quantum states is determined by the overlap of a relatively smooth neutron wave function with the scatterer profile); these difficulties remain when using the experimental installation and the methods described here.

4.2 Measurement of the parameters of low quantum states

The series of experiments was performed in [29] with a significantly better spectrometer resolution [34]. The methodological uncertainties in these experiments, as well as methods for further reducing them, were studied in detail. We note the particular features of the new experiment.

Advantages of the spectrometer were as follows.

(1) The precision and reliability in measuring the scatterer height were significantly increased due to the application of the capacitance method, such that corresponding uncertainties became negligible compared to the constraints imposed by quantum mechanics.

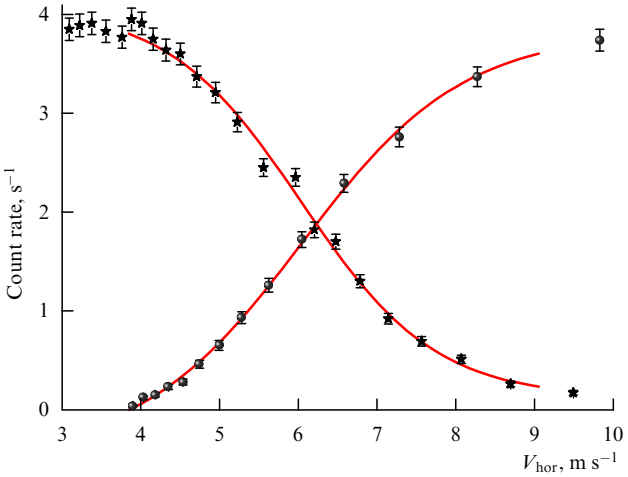

Figure 10. Measured spectrum of the neutron horizontal velocity components $V_{\rm hor}$. Circles correspond to the data measured using the top entrance collimator plate (the bottom plate is set to the smallest height). Stars indicate the data measured using the bottom entrance collimator plate (the top plate is set to the largest height). Solid lines stand for data approximation using the Boltzmann distribution.

(2) The statistical sensitivity of the new experiment was improved due to optimizing neutron transport in front of the spectrometer and due to the complete automation of this experiment.

(3) The background of the new neutron detector was even lower.

(4) New high-quality optical elements (mirrors and scatterers) were produced.

The spectrum of the neutron horizontal velocity components was measured in a way analogous to that in Ref. [28]. The method relies on a significant parabolic curvature of neutron trajectories in Earth's gravitational field. The measured spectrum of the velocity components $V_{\rm hor}$ is shown in Fig. 10. Both options of measuring the spectrum of the neutron horizontal velocity components, with top and bottom plates in the entrance collimator, yield analogous results. Measurements with a top plate in the collimator provide higher statistical accuracy for lower neutron velocities; measurements with a bottom plate result in higher statistical accuracy for higher neutron velocities.

The reflection of neutrons from mirrors was studied in experiments using several methods. Mirror waviness on rather large spatial scales was measured using light diffraction (if large, the mirror roughness would cause small-angle scattering of neutrons in the main experiment, and hence neutron escape from a quantum state). The mirror surface microroughness was measured using X-ray scattering (if large, the microroughness would scatter neutrons at large angles in the main experiment). Both measurements showed that the mirror quality was sufficiently high to exclude noticeable systematic errors in the experiment at the level of precision claimed. But the most direct and methodically transparent method consists in measuring specular reflection of neutrons; the neutron wavelength should be approximately equal to the wavelength used in the main experiment. As we have noted, the expected nonspecular reflection probability is small; therefore, it can hardly be measured in a single

reflection event. To enhance the observable effects of neutron loss from a specular trajectory, we passed a neutron beam through a narrow slit between two parallel mirrors at some angle to the mirror surface. This geometry provided many consecutive reflections of neutrons from the surface. If the probability of specular reflection is unity, then the neutron flux $F(\Delta z)$ is proportional to the slit size (with the quantum effects in the system neglected; this approximation is justified as long as the slit size is large enough). Any loss of neutrons from a specular trajectory would decrease the flux of neutrons passing through; in particular, if the slit size is small, the number of reflections is large. In the first approximation, the neutron flux is $F(\Delta z) = a\Delta z(1 - K_{\rm loss})^{L\varphi/\Delta z}$, where $K_{\rm loss}$ is the probability of neutron loss from a specular trajectory (assuming that the probability is independent of the incidence angle and the neutron velocity), L is the mirror length, φ is the mean angle of neutron incidence to the mirror surface, a is a normalization constant, and Δz is the slit size. Thus,

$$K_{\rm loss} = 1 - \left[\frac{F(\Delta z)}{a\Delta z}\right]^{\Delta z/(L\varphi)}.$$

The mirror on the bottom was a polished glass plate with the length $L = 12$ cm (used also in the main experiment). The mirror on the top was an analogous glass plate coated using magnetron sputtering with copper or a Ti–Zr–Gd layer 0.2 μm thick. The size of the slit between the mirrors was measured using the capacitance method. The slit size was set using piezo-translators in a way analogous to that used in the main experiment. The angle φ between the neutron beam axis and the mirror surface was 2.5×10^{-2} rad, which is sufficiently large to provide many consecutive collisions of neutrons with the mirror surfaces. The value $K_{\rm loss}$ for the glass surface did not exceed $(1.6 \pm 0.2) \times 10^{-2}$ per collision (even if specular reflection of neutrons from a copper surface was assumed), which is much smaller than the inverse number of consecutive collisions of neutrons with the bottom mirror in the main experiment (in the semiclassical approximation). In an analogous measurement with the mirror coated with a Ti–Zr–Gd layer, the probability of neutron loss from a specular trajectory was $(1.8 \pm 0.3) \times 10^{-2}$ per collision (assuming that the values $K_{\rm loss}$ for glass and gadolinium surfaces are equal). However, as is clear from a comparison with the previous experiment, neutrons were lost in the second experiment mainly because of their incomplete reflection from a mirror with an antireflecting coating. The probability of losing a neutron from the specular trajectory when the neutron is reflected from an antireflecting coating is about 3.5%. The small residual potential barrier of the coating was apparently large enough for total reflection of neutrons from the antireflecting coating. Even if the real part of the potential barrier is compensated precisely, the imaginary part of the potential would reflect neutrons efficiently; this is the so-called metallic reflection of neutrons from strongly absorbing materials [87].

The macroscopic flatness of all scatterers used was better than 0.5 μm; their surfaces were examined using standard methods, in particular with atomic force microscopes. The scatterer surface was coated with a thin layer of copper with the thickness 0.2 μm using magnetron sputtering. This coating was an upper electrode of the capacitor used to measure the distance between the mirror and the scatterer. The mean scatterer roughness (defined as the roughness amplitude distribution half-width at half-height) was equal to 0.7 μm. The roughness amplitude was smaller than in the first series of experiments; therefore, the scatterer efficiency was lower; however, the theoretical uncertainties in calculating its effective height were also smaller. This roughness amplitude is large enough for effectively scattering neutrons in nonspecular directions; nonspecular reflection increases the vertical neutron velocity component, thus increasing the frequency of neutron collisions with the mirror and scatterer and ensuring rapid neutron loss.

Our installation is a precision one-component gravitational neutron spectrometer. We consider the factors that determine its spatial resolution in the scanning neutron density mode using the scatterer.

(1) Fundamental factors, namely, the finite penetrability of the gravitational potential barrier separating classically allowed heights from the scatterer height. In other words, this is the finite sharpness of the Airy function describing the observation probability as a function of height. In addition, the resolution is constrained by the finite time of observing neutrons in the spectrometer.

(2) Finite accuracy of modeling the interaction of neutrons with the scatterer, especially related to deformation of the neutron wave functions by the scatterer.

(3) Methodical constraints, in particular, those caused by uncertainty in the absolute scatterer positioning and by the finite width of the neutron horizontal velocity component spectrum.

The first and second factors constraining the spectrometer resolution were considered in detail in Sections 3.3 and 3.4. The first factor smoothens the dependence $N(\Delta z)$, thus preventing the resolution of high quantum states, but it does not cause systematic shifts in estimating quantum state parameters. The second factor (unless a more accurate theoretical analysis [45–48] is used) could systematically shift the estimated values of the quantum state parameters. The corresponding systematic uncertainty in calculating the turning heights z_n for the lowest quantum states is ±1.5 μm.

It is interesting to estimate the minimum uncertainty in the neutron quantum state energy in our experiment following from the uncertainty principle. For this, we compare the time of observation of neutrons in the installation $\tau^{\rm pass}(V_{\rm hor})$ with the characteristic quantum mechanical interval $\Delta\tau_{\rm QM}$ equal to the ratio of the Planck constant to the neutron energy in the lowest quantum state, $\Delta\tau_{\rm QM} = \hbar/E_1 \approx 0.5$ ms. For the mean value of the neutron horizontal velocity 6.5 m s^{-1} (see Fig. 10), this ratio is $\tau^{\rm pass}(6.5\ {\rm m\ s^{-1}})/\Delta\tau_{\rm QM} \approx 30$; hence, the observation time in the considered experiment was long enough to ensure that the corresponding uncertainty is significantly lower than the measuring accuracy achieved.

We detail the uncertainties related to the accuracy in setting the scatterer height. The distance Δz between the mirror and the scatterer was measured using the capacitance method. Several metallic (aluminum) electrodes (2.0×1.5 cm each) were produced using magnetron sputtering on the flat glass surface on the bottom mirror. These electrodes and metallic coatings of a larger size (with the thickness 0.2 μm) on the bottom surface of the scatterer formed capacitances that were connected into *RC*-electric circuits such that they determined the oscillation frequencies of damped *RC*-generators. The oscillation frequency was uniquely related to the distance between the surfaces and was highly reproducible; the frequency as a function of the distance could be approximated rather precisely using a second-degree polynomial in the range 5 μm $< \Delta z <$ 1 mm.

Slits of an even smaller size are not transparent to neutrons anyway; besides, they could not be installed automatically due to the disturbance of dust particles between the mirror and the scatterer. If the distance is larger than 1 mm, then the capacity is too small and the sensitivity of the capacitor sensors decreases (such distances are not of interest for the performed experiments).

The unique relation between the *RC*-generator oscillation frequency and the distance between electrodes provides a high reproducibility of measuring the distance (much better than the required accuracy of about 1 μm); however, it is not sufficient for the precise measurement of the absolute distance. An additional procedure of absolute distance calibration was carried out following three independent methods using: (1) tungsten wire-spacers of a known diameter placed between the mirror and the scatterer; (2) a microscope with a long focal distance providing an optical image of the slit; (3) a precise mechanical device (comparator) measuring relative translations of some point on the upper surface of the scatterer. All these methods yielded self-consistent results. The use of the most precise method allowed calibrating the absolute size of the slit between the mirror and the scatterer with the accuracy ≈ 0.5 μm. But a difference in the surface areas of the electrodes and/or parasitic capacitances of the sensors caused different frequencies at equal heights with scattering in the range of $(5-7)\%$. Unfortunately, for simplicity of the measuring procedure, we had assumed that the sensors are equivalent; this assumption resulted in deviations from the scatterer parallel translation. The corresponding uncertainty Δz in height reached ± 1.0 μm when the slit size was $\Delta z \approx 15$ μm, and ± 1.6 μm when the slit size was $\Delta z \approx 25$ μm; this uncertainty was acceptable for the experiments performed.

We consider the experimental results. The neutron flux was measured as a function of the size of the slit between the mirror and the scatterer using a method analogous to that described in Section 4.1 (the difference consisted in a much higher accuracy of positioning of the optics elements, as well as in a higher statistical accuracy). In addition, the dependence of the neutron flux $F(\Delta z, V_{\text{hor}})$ in (16) on the neutron horizontal velocity component and on the type of scatterer/absorber was studied in greater detail. The study showed that the spectrometer spatial resolution could be improved by using a soft and more monochromatic spectrum of the velocity components V_{hor}. In the experiment, the mean amplitude of scatterer surface roughness was equal to 0.7 μm, i.e., it was smaller than that in the previous experiment described in Section 4.1 by about a factor of 1.5. A smaller roughness amplitude corresponds to a lower scatterer efficiency, and hence to a lower spectrometer resolution. Also, the study showed that the harder spectrum of neutron horizontal velocity components along the neutron beam direction corresponds to smaller values of the shift X, which is a free parameter in the simplified quantum mechanical model $F(\Delta z) \sim (\Delta z - X)^{3/2}$, assuming only one lowest quantum state and the classical asymptotic regime for a larger slit size. In this approximation, the values of X depends on the mean value $\overline{V}_{\text{hor}}$ as

$$\left(\frac{\partial X}{\partial(\tau^{\text{pass}}\,\overline{V}_{\text{hor}})}\right)^{\text{exp}}_{\tau^{\text{pass}}=15\text{ ms}} = 0.16 \pm 0.04\ \mu\text{m ms}^{-1}\,.$$

It is interesting to compare this measured value with theoretical expectations. For this, we estimate the sharpness of $F_1(\Delta z, V_{\text{hor}})$ as a function of its parameter V_{hor}, i.e., find the partial derivative $\partial F_1(\Delta z, V_{\text{hor}})/\partial(V_{\text{hor}})$. Numerical differentiation of Eqn (16) results in a value nearly insensitive to the other parameters of the problem, if the time of observation of a neutron in a quantum state is 15 ms:

$$\left(\frac{\partial X}{\partial(\tau^{\text{pass}})}\right)^{\text{theor}}_{\tau^{\text{pass}}=15\text{ ms}} = 0.2\ \mu\text{m ms}^{-1}\,;$$

the result reasonably agrees with the experimental data.

To improve the spectrometer spatial resolution (for fixed mirror and scatterer lengths) or to decrease the mirror and scatterer length (for a fixed spectrometer spatial resolution), we must study factors determining the scatterer efficiency. We considered two methods of spectrum shaping: (1) using an absorber produced from a material with a high cross section of absorption or inelastic thermal scattering of neutrons [7], and (2) using a scatterer with a rough surface, which scatters neutrons out of their specular trajectories [33].

The advantage of an absorber is the simplicity of estimating its height above the mirror, which is just the height of its lower flat surface. However, its efficiency is low: first, even an ideal absorber with a zero real part of its optical potential would reflect neutrons with the smallest energy because of the imaginary part of its optical potential; second, mixtures or alloys of materials with characteristic values of the real part of the optical potential about 10^{-7} eV does not result, in practice, in a uniform optical potential with the required small value about or smaller than 10^{-12} eV (this value is defined by the parameters of the neutron quantum states in Earth's gravitational field).

The scatterer in the second method (based on elastic nonspecular reflection of neutrons from its macroscopically flat and microscopically rough surface) allows overcoming the problem of low efficiency. It scatters neutrons in nonspecular directions with a probability close to unity (in the semiclassical approximation) if the amplitude of roughness of its surface is comparable to the characteristic scale z_0 of our quantum mechanical problem. But this constraint on the minimum roughness amplitude results in a difficult problem: the effective height of the scatterer above the mirror is no longer a well-defined value; with no adequate and precise theoretical analysis, the characteristic uncertainty of the scatterer height is about z_0 as well. A compromise solution can be found if a scatterer with a roughness amplitude sufficiently large for providing high scattering efficiency but significantly smaller than z_0 is used to provide a reliable value for the effective height of the scatterer above the mirror.

Taking the above arguments into account, we compared various absorbers and scatterers, in particular: (1) a rough scatterer with a copper coating; (2) an analogous rough scatterer with an antireflecting Ti–Zr–Gd coating. Results of measurements with these scatterers coincide within statistical accuracy. This coincidence means that the main scatterer property that ensures the loss of neutrons when it interacts with the surface consists in nonspecular neutron scattering on roughness rather than in neutron absorption. A summary result of this test is presented in Fig. 11.

We analyze the experimental results in the framework of the model of neutron tunneling through the gravitational barrier presented in Section 3.3. The solid line on the right in Fig. 11 is the result of approximating the experimental data using expressions (16) obtained in the model of neutron

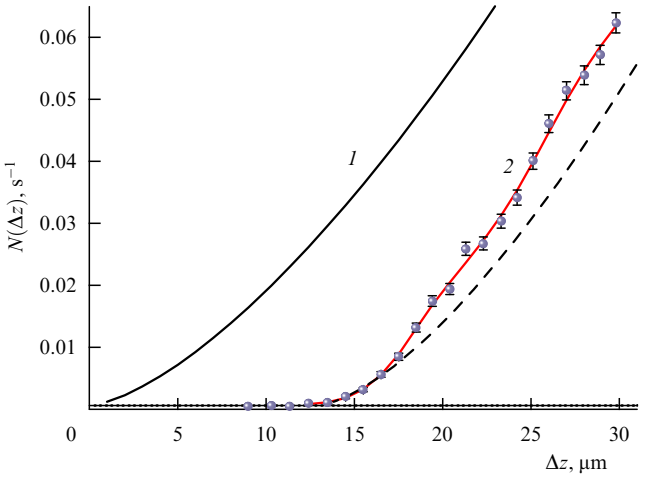

Figure 11. The neutron flux through the slit between the mirror and the scatterer is shown as a function of the scatterer height. Circles show summary data measured with copper and antireflecting Ti–Zr–Gd coatings. Line *1* corresponds to the classical model $N_{\rm cl}(\Delta z)$ normalized such that it approximates the experimental data at large scatterer heights. The dashed line stands for the simplified quantum mechanical model $N_{\rm QM,0}(\Delta z)$ assuming only one lowest quantum state and the asymptotic classical behavior $N_{\rm cl}(\Delta z)$ at larger scatterer heights. Line *2* approximates the experimental data using a quantum mechanical model in which the characteristic heights of the first and second quantum states z_1 and z_2, the lowest quantum state population, the normalization constant, and the scatterer efficiency are free parameters. Horizontal lines indicate the detector background value $\overline{V}_{\rm hor} = 4.9$ m s^{-1} and its uncertainties.

tunneling through a gravitational barrier. In this calculation, the characteristic quantum state heights $\{z_n, n > 2\}$ were assumed to be equal to the theoretical values for nonperturbed quantum states; the two lowest characteristic heights z_1 and z_2 were free parameters; the quantum state populations $\{\beta_n, n > 1\}$ were equal to unity; and the lowest quantum state population, the neutron flux normalization, and the scatterer efficiency were free parameters. This model approximates the experimental data with $\chi^2 = 0.9$.

A comparison of the presented model (assuming an infinitely high methodical spectrometer resolution) to the measured experimental data indicates that (1) the model approximates the data well within statistical uncertainties; (2) the lowest quantum state population ($\beta_1 \approx 0.7$) is lower than the populations of other quantum states (a similar observation was made after the first experiment considered in Section 4.1); (3) the first and second characteristic heights are $z_1 = 11.2$ μm and $z_2 = 20.2$ μm. The finite accuracy of measuring Δz respectively shifts the values z_1 and z_2 by 1.0 μm and 1.4 μm (because a decrease in the spectrometer spatial resolution mimics a decrease in the scatterer efficiency, resulting in a smoother behavior of the neutron flux as a function of the scatterer height, eventually leading to a false shift of the characteristic heights z_1 and z_2). As noted above, systematic uncertainties in estimating z_1 and z_2 result from a finite accuracy of the absolute calibration of the distance between the mirror and the scatterer (±1.0 μm and ±1.6 μm, respectively), as well as from a finite accuracy of the model description of the interaction of neutrons with the scatterer (with the uncertainty ±1.5 μm). The statistical uncertainty of measuring the characteristic heights z_1 and z_2 is ±0.7 μm, which is significantly smaller than the systematic uncertainties. The measured characteristic heights $z_1^{\rm exp} = 12.2 \pm 1.8_{\rm syst} \pm 0.7_{\rm stat}$ μm and $z_2^{\rm exp} = 21.6 \pm 2.2_{\rm syst} \pm 0.7_{\rm stat}$ μm agree with the expected values $z_1^{\rm theor} = 13.7$ μm and $z_2^{\rm theor} = 24.0$ μm within a statistical accuracy of 25%. As noted, the experimental values z_n may be slightly understated, unless a correction for deformation of the neutron wave functions is included explicitly. Hence, the expected spectrometer spatial resolution, as is clear from Fig. 11, agrees with the experimental data.

4.3 Measurements using position-sensitive detectors

The feasibility of the differential method using position-sensitive detectors was demonstrated in the experiment in [29]. This experiment was the first direct measurement of the neutron density distribution above a mirror; the spatial resolution was 1–2 μm. Comparison of the experimental data with theoretical estimates allows concluding, first, that the measured distribution of the probability of observing a neutron above the mirror agrees well with the theoretical expectation over the entire range of heights Δz, and second, that the detector spatial resolution could be estimated, for instance, using the sharpest part of the measured distribution around the zero height (the resolution is approximately equal to 1.5 μm); finally, even a relatively small variation in neutron density (about 10%) (expected for the mixture of several quantum states studied in this experiment) could be measured using the presented method.

Figure 12 shows experimental (a typical result of measurements over the course of a few days) and theoretical probability distributions of observing a neutron as a function of the height above the mirror, after passing a negative step of 21 μm. Evidently, our experimental method allows shaping and measuring the well-pronounced variation of the neutron density. The characteristic behavior of neutron wave functions in quantum states above the mirror and the successful

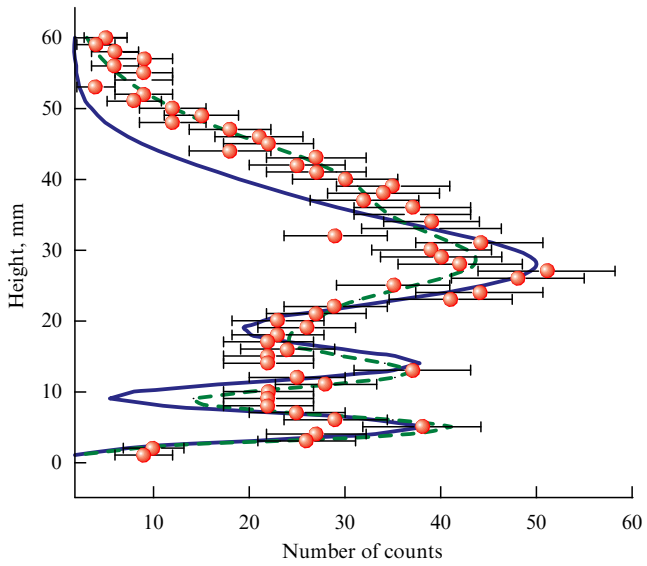

Figure 12. The neutron spatial density distribution in the gravitational field above a mirror is measured using a position-sensitive detector. Circles indicate the experimental data. The solid line shows the theoretical model assuming an ideal scatterer and no parasitic transitions between quantum states. The dashed line corresponds to a realistic finite scatterer efficiency. In both cases, precise neutron wave functions are used, and the quantum state populations are approximated from the experimental data. Interference between quantum states is neglected. The detector background is constant in the range from −3 mm to +3 mm above and below the range of height presented in this figure.

test of position-sensitive detectors with a uranium coating testify to the feasibility of experimentally identifying the gravitationally bound quantum states of neutrons using the method of direct measurement of the spatial distribution of their observation probability. We have measured, but not yet published, the data with a much greater supply of statistics.

We note that position-sensitive detectors could be used for measuring the distribution of neutron velocities in quantum states (5). For this, we should shift the detector by a few centimeters from the edge of the bottom mirror. The spatial distribution of neutrons measured in this configuration in a position-sensitive detector depends only on the neutron velocity distribution; any information on the neutron spatial distribution above the mirror is then lost. This method is considered in detail in Section 7 and in Ref. [30], where a similar method was used for observing and studying a related phenomenon: quantum states of neutrons in the effective centrifugal potential in the vicinity of a concave mirror surface. To measure the radial velocity distribution, we could use nuclear track detectors with the resolution ≈ 1 μm [34]; however, their spatial resolution is too high and the treatment procedure is too complex. We could also use position-sensitive detectors with the resolution ≈ 5 μm, which are currently being developed [83, 84], if the size of their sensitive surface increases to $\approx 5 \times 50$ cm. Finally, we could use more traditional position-sensitive linear stripe neutron detectors, for instance, those considered in Ref. [88], with the spatial resolution about 200 μm if the flight pass is adopted accordingly.

To summarize, both considered methods allow observing gravitationally bound quantum states of neutrons and measuring their characteristics with the currently available UCN fluxes.

5. Further prospects

Our theoretical formalism describing the interaction of UCNs with a scatterer and increasing the accuracy of the absolute scatterer positioning allows reaching the precision about 10^{-2} in measuring the parameters of the quantum states using the integral method. A similar accuracy can be achieved using the differential method based on position-sensitive detectors; an even higher precision can be obtained by measuring the vertical velocity distributions. Nevertheless, much more precise experiments are feasible if we succeed in using the method of resonant transitions between quantum states in a GRANIT spectrometer or interference between quantum states in analogy to measurements of the centrifugal quantum states of neutrons considered in Section 7.

Precision measurements require significant improvements in two related parameters: the energy resolution and the statistical accuracy. As follows from the energy–time uncertainty relation, the time of neutron storage in quantum states has to increase considerably in order to provide higher energy resolution. In the ideal case, the energy resolution can be as high as $\sim 10^{-18}$ eV if the observation time increases up to values comparable to the neutron lifetime (~ 15 min) determined by its β-decay. The 'flow-through' method is not appropriate for this purpose; instead, we have to close neutrons in a quantum trap, a box with the horizontal bottom and vertical side walls.

Preliminary analysis shows that significant progress in this direction is feasible. The critical parameter is the storage time of neutrons in the quantum state. Experimental analysis of the degree of specularity of neutron reflection from a surface is presented in Section 5.1. The energy of neutrons in the quantum states in such a trap can be calculated by measuring the frequency of resonant transitions between levels as described in Section 5.2, or the interference between the quantum states similarly to the method considered in Section 7 for the neutron whispering gallery wave.

The estimated frequencies of resonance transitions are quite convenient for experiments. The frequency of transition between the first and second level is about 256 Hz. Frequencies of some other transitions are given in Table 1. Resonant transition can be initiated in principle using various methods: mechanical oscillations of the quantum trap (accompanied by periodic variation of the height of one boundary trapping neutrons; this is a transition caused by the strong nuclear force); periodic variation of the height-dependent magnetic field gradient; and perhaps a periodic variation of the gravitational field, by means of a massive object rotating in the vicinity of the quantum trap. The last experiment is most difficult because of the weakness of gravitational interaction. However, it is interesting to estimate the feasibility of performing such an experiment using the existing or projected experimental installations and UCN densities. Various methods of inducing quantum transitions and estimations of the transition probabilities are presented in Section 5.2. The GRANIT spectrometer and

Table 1. The frequencies (in Hertz) of transitions between gravitational quantum states of neutrons above a mirror; n is the initial quantum state number and m is the final state number.

n \ m	1	2	3	4	5	6	7	8	9	10
1	0	256	465	650	818	975	1123	1264	1399	1529
2	256	0	209	393	562	719	867	1008	1143	1273
3	465	209	0	184	353	510	658	799	934	1064
4	650	393	184	0	168	325	474	614	749	879
5	818	562	353	168	0	157	305	446	581	711
6	975	719	510	325	157	0	148	289	424	554
7	1123	867	658	474	305	148	0	141	276	406
8	1264	1008	799	614	446	289	141	0	135	265
9	1399	1143	934	749	581	424	276	135	0	130
10	1529	1273	1064	879	711	554	406	265	130	0

a possible layout of an experiment using this spectrometer are described in Section 5.3.

5.1 Feasibility of a long-term storage of UCNs in specular trajectories

An important factor determining the precision of experiments using a GRANIT spectrometer is the time of storage of UCNs in quantum states. In the absence of external perturbations, quantum states are stable [89]. However, significant difficulty lies in the eventual mixing of large horizontal and small vertical velocity components caused by nonspecular reflection of UCNs from a surface. Precision measurement of the degree of specularity of UCN reflection is difficult without using the GRANIT spectrometer; however, preliminary tests using existing experimental equipment seem to be useful. We therefore performed a series of measurements of the specularity of UCN reflection from the surface of materials that could be considered candidates for use as the quantum trap in the GRANIT spectrometer [90, 91]. These measurements were also motivated by the development of neutron guides for efficient UCN transport.

Rectangular plates of synthetic monocrystal sapphire $10 \times 50 \times 50$ mm in size were used as a sample for the first measurement [90]. The surfaces to study were polished to the mean roughness amplitude ≈ 7 Å, measured using X-rays. The plate flatness was better than 1 μm. The measurement was performed using the gravitational spectrometer described in Ref. [34]. The scatter of UCN vertical velocity components was ± 0.07 m s^{-1} at the spectrometer exit; this value corresponds to the size ≈ 250 μm of the slit between the mirror and the scatterer. This UCN beam was sent through a long narrow slit between two vertical identical sapphire plates.

The mean angular scattering of the UCN horizontal velocity components at the entrance to the experimental setup was equal to $\pm 3°$; the angle between the sapphire plates and the initial neutron beam direction was 30°. The mean neutron velocity component along the neutron beam direction was ≈ 7 m s^{-1}. Defects in the plate edges were significantly smaller in size than the slit sizes used. When traveling through the slit between two parallel vertical plates, the neutron beam fell in the gravitational field by about 100 μm. The detector was installed such that its horizontal entrance collimation slit with the height about 5 mm was placed at the 'center of mass' of the incident neutron beam.

The total loss of neutrons per reflection (absorption, inelastic scattering, or elastic nonspecular reflection) is small; the first two loss channels are apparently negligible compared to the last one. The total loss probability was equal to $(0.4 \pm 0.9) \times 10^{-3}$ per collision. The estimated total neutron flux $F(\Delta x)$ through the slit, as a function of the slit size Δz, was $F(\Delta x) = a\Delta x(1-\mu)^{g(\varphi)/\Delta x}$, where μ is the total probability of UCN loss out of the specular trajectory per collision, φ is the angle between the neutron beam initial direction and the parallel sapphire plates, and a is a normalization coefficient. We note that the condition for specular reflection is defined here in a very conservative manner: UCNs are assumed to scatter specularly if the resulting angle deviation after multiple consecutive collisions (up to $\sim 10^3$ times) does not exceed 0.04 rad in the vertical plane. This angle corresponds to the size of a narrow horizontal collimation slit at the detector entrance. The mean neutron incidence angle corresponds to typical values in UCN neutron guides, as well as to the angles of UCN reflection from the side walls of the quantum GRANIT trap. But it is significantly larger than the angle of incidence to the bottom mirrors in the flow-through gravitational experiment, and therefore the probability of specular reflection in actual experiments is expected to be higher than the presented estimation. The UCN velocity is roughly equal to the characteristic values in all the presented cases. The sapphire surface was not treated additionally after polishing and standard cleaning of polishing powder and dust. The accuracy of setting the slit size and parallelism of the sapphire plates was no worse than a few micrometers. Measurements of neutron fluxes were repeated many times for each slit size in order to avoid systematic errors in setting the distances.

The results of these measurements allowed concluding that UCN reflection from a polished sapphire surface with the mean roughness amplitude 7 Å is highly specular; the probability of specular reflection is at least 99.8%. Such surfaces provide UCN transport with minor losses over the distance 25–100 m through neutron guides with the cross section 5–10 cm. Preliminary data on the measurement of the high probability of specular UCN reflection, 99.9(1)%, from a Ni replica surface were reported in Ref. [92]. If all the other parameters are the same, the advantage of the Ni surface consists in a higher critical velocity, 7 m s^{-1}. Such UCN transport on specular trajectories provides a new quality: first, UCNs could be transported from a neutron source to an experimental setup with minor losses; second, we can consider neutron transport from a reactor or spallation source hall to a special laboratory with low background and smaller spatial constraints [93]; third, specular sapphire neutron guides provide an elegant solution for extracting UCNs from pulsed sources [94–96]; finally, and most importantly for experiments with gravitational neutron states, the time of storage of UCNs in the quantum trap in the GRANIT spectrometer can be rather high.

The second measurement [91] was carried out in the same setup with the same parameters, but the statistical accuracy and quality of the sample mirrors were higher. We compared the following mirrors: optical glass, sapphire, and glass with a diamond-like coating (DLC) or copper coating. The choice of materials was determined as follows:

(1) The value of the critical velocity of the bottom mirror material is not important because the neutron incidence angle is too small; therefore, optical glass with no coating is an interesting candidate.

(2) The value of the critical velocity of the vertical side mirrors is extremely important because it determines the number of neutrons accumulated in the quantum trap for a given phase space density. For this application, diamond-like or isotopic copper coatings can be interesting.

(3) If the above options are not available, a compromise solution could be to use sapphire.

All samples were studied carefully using neutron and nonneutron techniques. The relative square area of defects did not exceed 10^{-6} for any of the samples except the copper one. The roughness amplitude was equal to 0.5–0.8 Å for all glass with and without coatings; the roughness amplitude for sapphire was chosen large enough in order to easily measure the effect of roughness on neutron data. The respective flatness of the glass mirror, the glass with copper coating, and the glass with diamond-like coating was 80, 100, and 220 nm (in the last case, the larger roughness is due to the strong stress in the diamond-like coating). The coating thickness was 200 nm. When choosing a procedure to apply

the coatings, we took into account that the application of hydrogen-containing materials used in chemical methods (chemically vapor-deposited, CVD) must be limited. We studied two techniques in experiments: radio-frequency magnetron sputtering and ion beam sputtering (IBS). In the first case, the layer growth rate was small and the layer adhesion was weak. Therefore, we selected the second technique for making the diamond-like coating and the first technique to test the copper coating. The copper coating had visibly degraded before starting the neutron measurements.

The measured total probability of neutron loss from a specular trajectory was $(0.5 \pm 0.2_{\text{stat}} \pm 0.2_{\text{syst}}) \times 10^{-3}$ for glass, $(4.0 \pm 0.4_{\text{stat}} \pm 0.2_{\text{syst}}) \times 10^{-3}$ for diamond-like coating, $(6.1 \pm 0.6_{\text{stat}} \pm 0.2_{\text{syst}}) \times 10^{-3}$ for the sapphire, and $(15.9 \pm 4.0_{\text{stat}} \pm 0.3_{\text{syst}}) \times 10^{-3}$ for the copper coating. The systematic uncertainties are determined by the accuracy in positioning the mirrors. The equality of statistical and systematic uncertainties for the best surfaces indicates that the accuracy cannot be easily improved when using the present measuring method. However, this accuracy is good enough for making a justified conclusion on the mirror quality and on the choice of material for the GRANIT trap. The high quality of all surfaces investigated allows using them at the first stage of the GRANIT experiment. The bottom mirror could be made of optical glass; however, any mechanical motions in the vicinity of sharp edges of such a mirror must be avoided in view of their fragility. A large bottom mirror with the size 30×30 cm cannot currently be made of sapphire. The side walls of the quantum trap could be built of optical glass with a diamond-like coating. Nevertheless, we note that the nonzero probability of nonspecular reflection found for the diamond-like coating is related to the coating inhomogeneity rather than to its surface roughness. Therefore, we can hope to improve this parameter in the future, albeit through expending significant technological efforts.

Other factors that limit the time of neutron storage in quantum states, mainly due to the mixing of horizontal and vertical velocity components, were studied theoretically [97]; their experimental analysis will be possible only with the GRANIT spectrometer. These factors are the nonverticality of the quantum trap side walls, the waviness of the mirrors, the defects of the mirror edges, and vibrations. The effect of Earth's rotation on gravitational quantum states [98–100] also decreases the time of neutron storage in quantum states; analogous effects were earlier observed in the experiment measuring the gravitational phase shift in neutron interferometers [101]. Neither of these effects manifests itself in the flow-through measuring mode because the observation times were too low, while the storage times in the accumulation measuring is apparently limited by the precision of the production and installation of the mirrors, by the accuracy of setting the vertical side walls, and by the defects of the mirror edges. Partial times of neutron storage as a function of the quantum state number are presented in Fig. 13 [97]; they correspond to each presented effect.

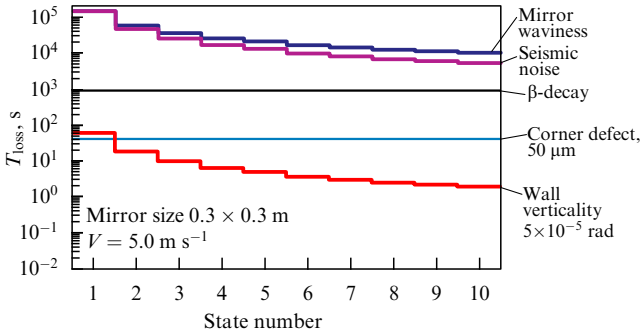

Figure 13. Partial times of storage of neutrons in gravitational quantum states are estimated as a function of the quantum state number. The corresponding effects are: mirror waviness analogous to that measured in Ref. [102] for a silicon mirror, vibrations of the mirror equal to seismic noise, neutron β-decay, defects of 50 μm in the horizontal mirror edges, nonverticality of the side walls (5×10^{-5} rad).

5.2 Resonant transitions between gravitational quantum states

The rather low frequencies of quantum transitions (about $f_0 = 145$ Hz) in principle allow inducing the transitions using various methods. The theoretical results listed in this section describe transitions between quantum states induced by a harmonic perturbation following the formalism given in Ref. [43], which is based on the general formalism in [20].

The differential equation

$$\mathrm{i}\hbar \frac{\mathrm{d}a_m}{\mathrm{d}t} = \sum_k V_{mk}(t)\, a_k \tag{18}$$

with the matrix element $V_{mk}(t) = \int \Psi_m^{*(0)} V(t) \Psi_k^{(0)}\, \mathrm{d}z$ describes the evolution of our quantum system; here, $\Psi_n^{(0)}$ are solutions of the nonperturbed Schrödinger equation, $V(t)$ is the harmonic perturbation, $V(t) = V_0(z) \exp(\mathrm{i}\omega t) + V_0(z) \exp(-\mathrm{i}\omega t)$, with the factor $V_0(z)$ depending on the height z. We note that quantum transitions are not induced by a perturbation if it is independent of the height z. If the system is initially $(t = 0)$ in the ground state $(a_1(0) = 1; \{a_m(0) = 0, \forall\, m \neq 1\})$, then the probability of observing it in a state n at the instant t is $P_n(t) = |a_n(t)|^2$. If the perturbation frequency ω is close to the resonance frequency $\omega_{n0} = (E_n^{(0)} - E_1^{(0)})/\hbar$, i.e., the difference $\varepsilon = \omega_{n1} - \omega$ is small, then the transition matrix element is

$$V_{n1}(t) = \int \Psi_n^{*(0)} V(t) \Psi_1^{(0)}\, \mathrm{d}z \approx \exp(\mathrm{i}\varepsilon t) \int \psi_n^* V_0(0) \psi_1\, \mathrm{d}z = F_{n1} \exp(\mathrm{i}\varepsilon t)\,, \tag{19}$$

and the probability of observing the system in the nth excited state is

$$P_n(t) = |a_n(t)|^2 = \frac{\Omega_0^2}{\Omega^2} \sin^2(\Omega t)\,, \tag{20}$$

where $\Omega_0 = F_{n1}/\hbar$ and $\Omega^2 = \Omega_0^2 + \varepsilon^2/4$. This is the Rabi formula corresponding to the oscillations of a system between two coupled states; the oscillation frequency is 2Ω. The probability of observing a neutron in the excited state oscillates between the values 0 and Ω_0^2/Ω^2. The maximum probability depends on the perturbation frequency in a resonant manner:

$$P_{\max}(\omega) = \frac{\Omega_0^2}{\Omega^2} = \frac{(2F_{n1})^2/\hbar^2}{(\omega - \omega_{n1})^2 + (2F_{n1})^2/\hbar^2}\,. \tag{21}$$

The resonance width Γ_n is defined by the perturbation matrix element F_{n1}: $\Gamma_n = 4F_{n1}$. Two neighboring states, n and $n+1$, are resolved if the difference in their energies is larger

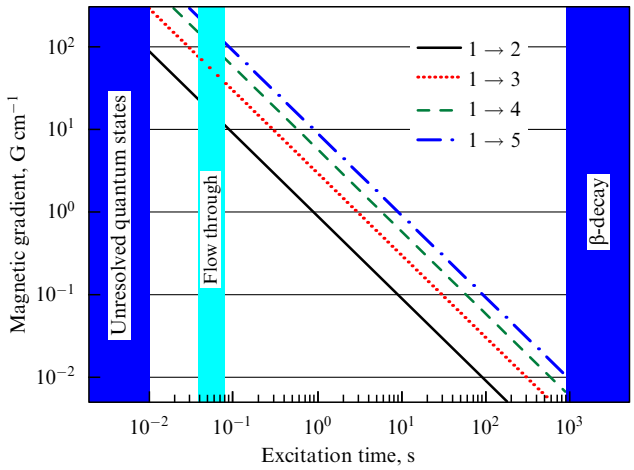

Figure 14. The strength of the vertical magnetic field gradient needed for providing the maximum resonance transition probability is estimated as a function of the perturbation time for the transitions $1 \to 2$, $1 \to 3$, $1 \to 4$, and $1 \to 5$. Vertical broad lines indicate the perturbation times corresponding to unresolved quantum states, the time of flight of neutrons above the mirror in the flow-through mode, and the neutron lifetime.

than the corresponding width,

$$\Delta E_{n+1,n} = \hbar\omega_{n+1,n} > \Gamma_n \,,$$

i.e., the matrix element F_{n1} is not too large. The excited quantum state population at the resonance $\varepsilon = 0$ evolves as $P_n(t) = \sin^2(\Omega_0 t)$. The transition probability is large for the transition time $\tau \approx \hbar/F_{n1}$. Combining these two conditions, we conclude that the neutron observation time has to be lower than $4/\omega_{n+1,n}$ for observing the resonant transition. For instance, for the transition between the ground state ($n = 1$) and first excited state ($n = 2$), the corresponding frequency has to be equal to 256 Hz, and $\tau > 4$ ms. For neighboring quantum states in some excited spectral range, the time τ has to be larger than that as the difference in energy between neighboring states decreases when the quantum number n increases.

We consider transitions induced by the magnetic field

$$\mathbf{B} = (\beta_z \mathbf{e}_z + \beta_x \mathbf{e}_x)\, z \cos(\omega t) \qquad (22)$$

interacting with the neutron magnetic moment $\boldsymbol{\mu}$, $V(t) = -\boldsymbol{\mu}\mathbf{B}$. Because the uniform magnetic field does not mix two quantum states, we need a nonzero magnetic field gradient. We neglect the components $(\beta_x \mathbf{e}_z - \beta_z \mathbf{e}_x)\, x \cos(\omega t)$ that do not induce quantum transitions. A quantum transition with no spin-flip can be induced due to the first term in Eqn (22) with the perturbation $V_{\text{non-flip}}(t) = -\mu_z \beta_z z \cos(\omega t)$. Then the interaction matrix element is $F_{n1} = \mu\beta_z z_{n1}$, where μ is the neutron magnetic moment and $z_{n1} = \int \psi_n^* z \psi_1 \, \mathrm{d}z$. The last value can be calculated numerically, for instance, $z_{21} = 0.653 z_0$ for $n = 2$. The magnetic field gradient needed for a neutron transiting between the two lowest quantum states with a probability close to unity is $\beta_z = \hbar/(\mu z_{12} t)$. In a more general case, the characteristic parameters of the problem are shown in Fig. 14. The quantum transition accompanied by a spin flip is induced due to the second term in Eqn (22) with the perturbation $V_{\text{flip}}(t) = -\mu_x \beta_x z \cos(\omega t)$. In accordance with the Maxwell equations, both terms are present simultaneously in any field configuration. Therefore, we have to take into account or reduce the effects caused by the Zeeman magnetic level splitting in order to obtain precise values for gravitational quantum state energies. There are at least three options: (1) if the magnetic perturbation is small and the quantum transition time is large, the Zeeman splitting is small. For example, the magnetic contribution to the energy of the levels is smaller than 10% if the constant magnetic field component is smaller than 1 μT; (2) if the uniform vertical magnetic field with the strength ~ 100 μT is applied, then quantum states with equal gravitational and different magnetic quantum numbers are split by ~ 10 peV, which is significantly larger than the characteristic gravitational energy ε_0, and hence the transition probability is considerably suppressed; (3) an analysis of neutron polarization before and after the transition allows separating the two types of transitions.

Transitions between quantum states could be induced by mechanical harmonic oscillations of the mirror with the amplitude δz in analogy to those observed in Ref. [104]. Such oscillations correspond to the periodically oscillating boundary condition in Schrödinger equation (1):

$$\psi\big(z = \delta z \cos(\omega t)\big) = 0 \,. \qquad (23)$$

As shown in Ref. [43] in analogy to Ref. [105], in the limit of a small perturbation, this problem reduces to that with a fixed boundary condition and small perturbation potential. Moreover, the oscillation amplitude needed for providing the maximum resonance transition probability for the time τ [s] is $\delta z = 20$ nm/τ [s]; it is independent of the pair of states involved in this transition.

The most curious type of transition is that induced by a gravitational field; the field could be, for instance, modulated using a massive body rotating in the vicinity of the experimental setup. An evident complication of such an experiment is related to the gravitational interaction weakness. As shown in Ref. [43], the transition matrix element is $F_{21} = 0.77GmMz_{21}/L^2$. Even if the neutron observation time equals its β-decay lifetime and the characteristic size of the oscillating body is $L = 20$ cm and its density $\rho = 20$ g cm^{-3}, the transition probability is small: $\sim 10^{-4}$. Nevertheless, the probability increases, for instance, for two neighboring highly excited quantum states. It can be shown that the matrix element $z_{n+1,n}$ behaves as $z_{n+1,n} \sim n^{2/3}$ for $n \gg 1$, i.e., it increases sharply as n increases, while the transition frequency decreases: $\omega_{n+1,n} \sim n^{-1/3}$. These arguments simplify realization of such an experiment.

Moreover, the sensitivity increases considerably in interferometric experiments, in which transitions are induced by the common action of two different reasons: for instance, by harmonically varying the magnetic field gradient and by rotating the mass. The matrix element F_{nk} for such a transition is equal to the sum of large F_{nk}^{large} (for instance, magnetic or mechanical) and small F_{nk}^{small} (gravitational) terms:

$$F_{nk} = F_{nk}^{\text{large}} + F_{nk}^{\text{small}} \,. \qquad (24)$$

The transition probability can be presented as a function of the relative phase of these two perturbations:

$$P_+(t) \approx |F_{nk}|^2 \approx |F_{nk}^{\text{large}}|^2 + 2F_{nk}^{\text{small}} F_{nk}^{\text{large}} \quad \text{or}$$
$$P_-(t) \approx |F_{nk}^{\text{large}}|^2 - 2F_{nk}^{\text{small}} F_{nk}^{\text{large}} \,. \qquad (25)$$

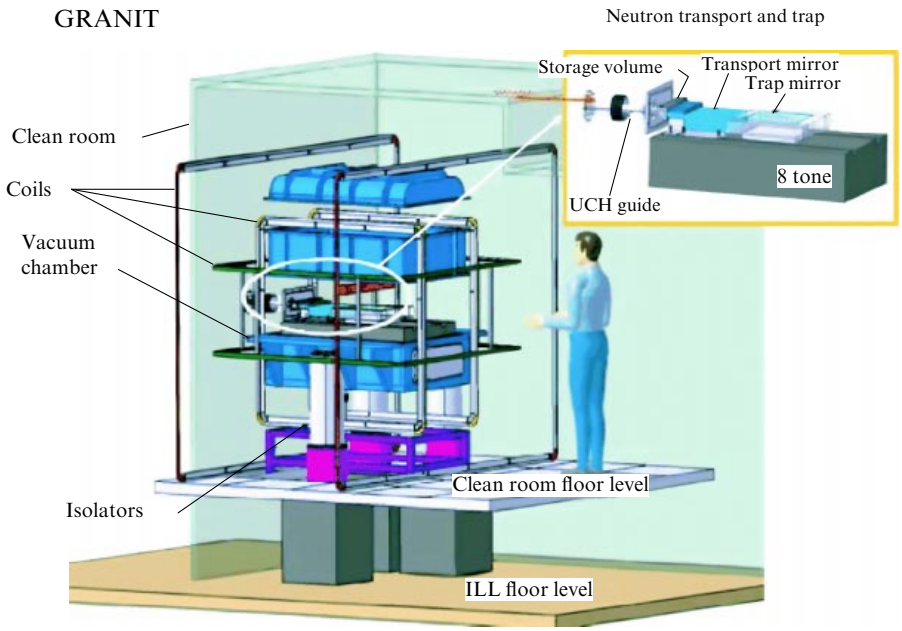

Figure 15. GRANIT spectrometer.

Hence, the asymmetry is

$$A = \frac{P_+(t) - P_-(t)}{P_+(t) + P_-(t)} \approx 2\left|\frac{F_{nk}^{\text{small}}}{F_{nk}^{\text{large}}}\right|. \qquad (26)$$

Based on estimates given above, we can conclude that the measurement of resonance transitions induced by the joint action of a strong harmonic perturbation and a weak gravitational field are possible in principle.

5.3 GRANIT spectrometer

The GRANIT spectrometer is a new-generation experimental installation under construction currently at ILL, Grenoble. It aims at studies of most of the questions described in this review. All the important parameters of the GRANIT spectrometer are improved by several orders of magnitude compared to those achieved in the preceding gravitational spectrometer [34]. GRANIT will allow increasing the accuracy for measuring parameters of gravitational quantum states due to a longer storage of UCNs in quantum states [43, 97] and due to a higher number of statistics [106–108]. The quantum state energies will be measured using resonance transitions between quantum states and using oscillations between quantum states [30, 43, 103]. The GRANIT spectrometer is being installed as a permanent experimental installation in level C at the ILL reactor in Grenoble, in the framework of an ANR (Agence Nationale de la Recherche, France) grant [109] supported by ILL and IN2P3 institutes. Among the new techniques in the experimental program considered for this spectrometer, we note using polarization analysis and real-time position-sensitive detectors. The GRANIT spectrometer is shown in Fig. 15 in its simplest configuration.

The following systems are installed on a granite plate inside a vacuum chamber:

(1) A system of neutron guides that connects an ^{4}He UCN source [106] to the spectrometer via an intermediate storage volume. The mechanical flexibility of the transport system allows protecting the spectrometer against neutron source vibrations.

(2) A semi-diffusive narrow slit with the height 100–200 μm [107, 108] at the intermediate storage volume exit allows extracting only the UCNs with small vertical velocity components. Other UCNs are reflected back by the slit; thus, UCN phase space density does not decrease.

(3) A transport mirror at the semi-diffusive slit exit. It consists of a horizontal and two vertical mirrors, as well as of a scatterer above the horizontal mirror.

(4) A rectangular mirror with the size 30 × 30 cm and four vertical side mirrors as the principal element of the spectrometer allowing long UCN storage in quantum states.

(5) A system of wires with the electric current above the horizontal transport mirror (it is shown in more detail in Fig. 16); it provides resonant transitions between quantum states in the flow-through measuring mode.

(6) Detectors of three types to be used at the first stage: ^{3}He-gaseous proportional counters with extremely low backgrounds for integral measurements, position-sensitive nuclear-track detectors [29, 34] with the spatial resolution about 1 μm for the differential measurements, and real-time position-sensitive detectors with the spatial resolution $\sim$ 100 μm for measuring neutron velocity distributions.

(7) Numerous devices for spectrum shaping and analyzing, and also for precision positioning to be used whenever needed.

Outside the vacuum chamber, two main systems protect the spectrometer from external perturbations:

(1) an anti-vibration and leveling system is built as follows. The first level of spectrometer protection against vibrations and its approximate leveling are provided by three pneumatic cylindrical legs with active valves; these legs support the vacuum chamber. Another level of anti-vibration protection and precise leveling of the installation is provided by three piezo-element legs placed inside the vacuum chamber. A granite plate with many spectrometer components on it is installed on these three legs. Thus, the

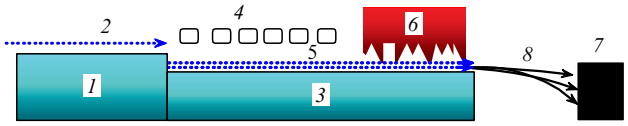

Figure 16. Schematic of the magnetic excitation of resonant transitions between gravitational quantum states of UCNs in the flow-through mode in the GRANIT spectrometer. All low-lying gravitational quantum states are populated above mirror *1*. The motion of neutrons above this mirror is shown schematically with dotted line *2*. A small negative step with the height ≈ 20 μm between mirrors *1* and *3* allows populating only excited quantum states above mirror *3*. Quantum transition between an excited and the lowest gravitational quantum state is provided due to a magnetic field gradient periodically varying in space. The magnetic field is induced by a current in wires *4*; the current has the opposite sign for all neighboring wires; the current (of a few amperes) is adjusted in order to provide the maximum probability of quantum transition. The spatial period of the magnetic field gradient variation is about 1 cm. In the reference frame of a moving neutron, this spatial periodicity of the magnetic field gradient is seen as its variation in time, and the perturbation frequency is proportional to the horizontal neutron velocity. The quantum motion of neutrons above mirror *3* is illustrated schematically with dotted line *5*. Scatterer *6* selects the lowest quantum state and eliminates all excited states. The classical neutron parabolic trajectories between the exit from mirror *3* and position-sensitive detector *7* are indicated with solid lines *8*. Using the height of the neutron detection, one can calculate the neutron horizontal velocity component.

spectrometer is reliably isolated from vibrations coming from the reactor hall floor. Residual vibrations will apparently come from the neutron source through mechanical connections;

(2) a clean room protects the sensitive optical elements of the spectrometer. First, mechanical adjustments of any two mirrors with the characteristic accuracy ~ 1 μm are possible only if the size of all residual dust particles is smaller than that. Second, hard dust particles would damage the mirrors if they fall into so narrow a gap. That is why the spectrometer is placed inside the clean room. The air flux in the central part of the clean room, where the spectrometer with delicate optical elements is installed, is laminar.

Here, we do not detail the efforts devoted to increasing the UCN density needed for improving the statistical accuracy of experiments. We only note that we are considering all known options: a solid-deuterium UCN source in the vicinity of a cold neutron source inside the ILL reactor [110] and a helium UCN source in the H172 external cold neutron beam at ILL [106]. We are developing an original scheme for extracting UCNs from such a helium source [107, 108], as well as nanopowder reflectors analogous to those described in Ref. [112] for increasing the fluxes of neutrons with the wavelength 8.9 Å in the source. We are exploring novel principles for producing UCNs based on thermalization of very cold neutrons in gels of ultracold nanoparticles [113–116]. In the GRANIT project, high phase-space UCN density will be achieved through the construction of a specialized cold neutron guide, a monochromator for neutrons with the wavelength 8.9 Å, and an ^{4}He UCN source. Cold neutrons with a broad velocity distribution are produced in the vertical cold neutron source in the ILL reactor. They are transported through the H172 neutron guide to the neutron monochromator, which consists of 18 crystals of intercalated graphite $C_{24}K$ with the mosaicity $1-2\%$ and is installed at the distance 12 m from the cold neutron source. The monochromator reflects cold neutrons with the wavelength 8.9 Å at the angle 61.2° to a secondary neutron guide 4.5 m long coated with an $m = 2$ supermirror. The UCN source is installed at the neutron guide exit; a specialized system extracts UCNs with no major loss of UCNs in phase space. A system of transport neutron guides delivers UCNs to the GRANIT spectrometer located inside the clean room.

The main contribution to the UCN density in helium sources comes from neutrons with a narrow distribution of wavelengths around 8.9 Å. Therefore, just such neutrons are selected using the mentioned intercalated graphite monochromator [117, 118] and are delivered through the secondary neutron guide to the UCN source. Losses in the UCN density in the source are caused by imperfections in the monochromator and the neutron guides, as well as by the absence of a multiphonon contribution to UCN production [119]. However, the choice of the presented configuration is justified by a much better background suppression compared to that with a UCN source installed directly in a white cold neutron beam. The optimum parameters of the UCN source are presented in Ref. [106].

An experiment with the GRANIT spectrometer will study resonance transitions between gravitational quantum states induced by a periodic spatial variation of the magnetic field gradient [103]. If the perturbation frequency in the reference frame of a moving neutron coincides with the quantum transition resonance frequency, the transition probability increases sharply. The principle of observation is explained in the caption to Fig. 16.

The neutron flux through the slit between mirror *3* (see Fig. 16) and the scatterer is defined by the lowest quantum state population if the scatterer is raised to a corresponding height. In the absence of resonant transitions, the population of this quantum state is zero. Otherwise, the neutron flux through the slit and the horizontal components of their velocity can be measured using the fact that neutrons with different velocities fall to different heights in the gravitational field when passing interval *8* in Fig. 16. With a known velocity, we can calculate the quantum transition frequency, and hence the difference in energy of the corresponding states. Knowing the differential neutron fluxes at the spectrometer entrance and exit, we can estimate the quantum transition probability. The optimum parameters of such an experiment are given in Ref. [100].

6. Gravitational quantum states of neutrons versus other physical phenomena

Neutron gravitational quantum states can be used in fundamental and applied physics, because this is an a priori very clean system with quantum state energies and wave functions defined only by the interaction of neutrons with a gravitational field; they are independent of the properties of the experimental installation.

For instance, interesting constraints on fundamental short-range forces (Section 6.1), on axion-like interactions (Section 6.2), and on the electric neutron charge (Section 6.3) can be obtained using neutron gravitational quantum states. The observation of the evolution of localized neutron wave packets (presented in Section 6.1) is interesting in and of itself, but it also serves to measure storage times of neutrons in quantum states. A broad subject for studies is the interaction of neutrons in a quantum state with the gravitational field (Section 6.5). The phenomenon of gravitational neutron states has methodical applications: studies of surface layers,

efficient neutron transport, UCN extraction from ^{4}He sources with no major loss in the UCN density, neutron-tight valves (Section 6.6), and so on.

6.1 Constraints on additional short-range forces

In accordance with the predictions of the grand unified, supersymmetric, supergravity, and superstring theories, there should be a set of additional light particles [120]. Due to the exchange of such particles between masses, there should be additional short-range forces. The intense study of such forces in recent years was motivated in particular by the hypothesis of 'large extra spatial dimensions' proposed by Antoniadis, Arkani-Hamed, Dimopoulos, and Dvali [121–123] based on earlier ideas in [124–130]. If the number of extra dimensions is $n = 2$, the characteristic interaction range is a few micrometers; if it is $n = 3$, the interaction range is a few nanometers [121, 131]. A review of theoretical hypotheses and experimental results is presented, for instance, in Refs [132–138]. These hypotheses could be verified using neutrons because false electromagnetic effects are significantly suppressed because neutrons are electrically neutral [131, 139–149]. The effective gravitational interaction is usually parameterized in the presence of an additional Yukawa-type force as

$$V_{\rm eff}(r) = G\,\frac{m_1 m_2}{r}\left[1 + \alpha_G \exp\left(-\frac{r}{\lambda}\right)\right], \qquad (27)$$

where G is the Newton gravitational constant, m_1 and m_2 are the interacting masses, r is the distance between them, and α_G and λ are the intensity and the characteristic scale of the hypothetical interaction.

If an additional short-range interaction between neutrons and the mirror existed in Ref. [29], the parameters of the gravitational quantum states would change. The interaction between neutrons and Earth is described by the first term in Eqn (27): $V(z) = mgz$, where $g = GMm/R^2$ $(r = R + z)$, R is Earth's radius, and M is its mass. The second term stands for an additional interaction. Due to the smallness of the characteristic range λ, the leading contribution of an additional interaction comes from the neutron interaction with a thin layer of the mirror surface (and with a scatterer to a much smaller extent). An additional potential of the attractive interaction between neutrons and the mirror is

$$V_{\rm Y}(z) = -U_0 \exp\left(-\frac{z}{\lambda}\right) \qquad (28)$$

in the limit of small λ; here, $U_0 = 2\pi G\alpha_G m\rho_{\rm m}\lambda^2$ and $\rho_{\rm m}$ is the mirror density.

The first attempt at setting a model-dependent constraint for short-range forces in the distance range $1-10$ μm obtained from our experiments was undertaken in Ref. [142]. A model-independent but rough constraint for the additional interaction strength follows from the condition that it does not form an extra quantum state [143]: $\alpha_G = 10^{15}/\lambda\,[\mu{\rm m}]$. This constraint could be improved by a few times, for instance, due to another choice of a higher-density mirror material (or coating); additional improvement by an order of magnitude could be achieved by increasing the accuracy of measurements in the flow-through mode. However, even in this case, the constraint would still be worse than the current limits.

Nevertheless, an interesting improvement by many orders of magnitude is feasible using long neutron storage in the GRANIT spectrometer trap; the optimum sensitivity could be achieved in the vicinity of the characteristic quantum mechanical scale z_0 of the problem. The improvement factor around z_0 is larger than $\tau_{\rm m}/\tau_{\rm QM}$, where $\tau_{\rm m}$ is the lifetime of the most long-lived quantum state, and $\tau_{\rm QM} \approx 0.5$ ms. This factor defines the quality factor (relative width) of the resonant transition between quantum states. In addition, the analysis of the resonant curve shape allows increasing the accuracy even further. The expected time of storage of neutrons in quantum states, equal to 1 s at the first stage in the GRANIT experiment, provides the improvement factor $\sim 10^3$. Measurement of the resonance shape with an accuracy of 1% would increase the constraint sensitivity by another factor $\sim 10^2$. However, we refrain from making such a far-reaching extrapolation of the sensitivity until a more reliable estimate is offered by the next stage of the experiment.

In some models, a power law for the interaction strength as a function of the distance is considered instead of Yukawa-type interaction (27). It is shown in [150] that the sensitivity of experiments with gravitational quantum states to additional interactions is not high.

Another sensitive method of searching for short-range interactions using neutrons could be provided by studies of the quantum states of slow neutrons in the vicinity of a concave mirror. This problem is considered in Section 7. In mathematical terms, it reduces to the problem of neutron gravitational quantum states above a mirror; here, centrifugal force plays the role of gravity. The characteristic energies and sizes of neutron wave functions strongly differ: the quantum state energy is around the mirror material optical potential, and the radial neutron wavelength is about a few dozen nanometers. This characteristic scale defines the length of the maximum sensitivity of the method. The accurate analysis of the sensitivity of this method has not yet been carried out; therefore, we can just discuss preliminary estimations.

But the most interesting neutron constraint is obtained in the nanometer range using the method of angular analysis of neutrons scattered on nuclei [148]. The rather high sensitivity of such experiments to short-range forces is explained as follows. In the center-of-mass reference frames, the scattering amplitude for slow enough neutrons in atoms could be expressed with good approximation as $f(q) = f_{\rm nucl}(q) + f_{\rm ne}(q) + f_{\rm Y}(q)$. Here, $f_{\rm nucl}(q)$ is the neutron–nucleus amplitude of isotropic and energy-independent scattering described with a single parameter, the scattering length $b = -f_{\rm nucl}(q)$ [151]. The small energy-dependent electromagnetic term $f_{\rm ne}(q)$, due to the interaction between the electric charge distribution inside the neutron and the atomic electric charge distribution, provides a slight asymmetry of scattering. Finally,

$$f_{\rm Y}(q) = -A\,\frac{q^2}{4\pi}\,\hbar c\,\frac{2m\lambda^2/\hbar^2}{1 + (q\lambda)^2}$$

is the scattering amplitude caused by an additional interaction. The scattering amplitude $f_{\rm Y}(q)$ would cause an asymmetry in neutron scattering if the neutron wavelength were smaller than the characteristic interaction radius; this idea was used for setting the constraint. Probably the best way of further improving the sensitivity is precisely measuring the angular distributions of cold and very cold neutrons in atoms of a diluted inertial gas (for instance, argon or helium) as a function of the neutron wavelength [148]. In such an experiment, an asymmetry in neutron scattering due to the contribution of the amplitude $f_{\rm ne}(q)$ does not appear as long

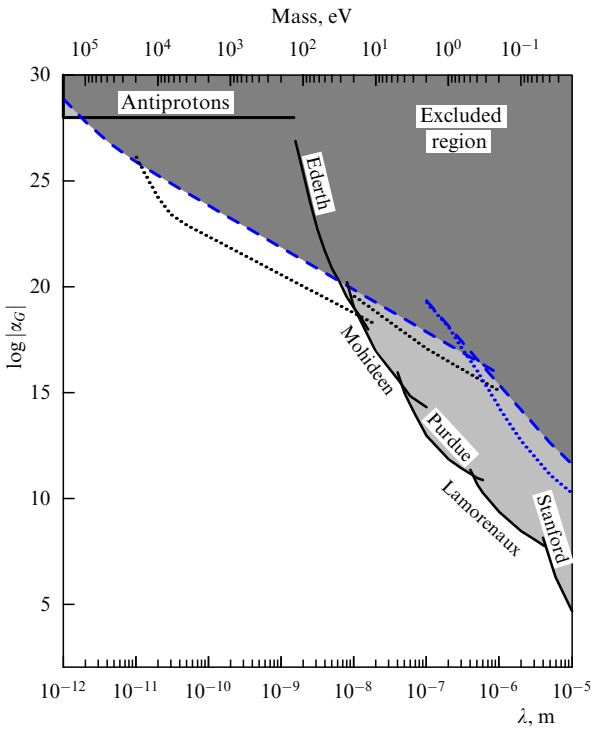

Figure 17. The best constraints for the strength α_G of an additional short-range interaction are shown by the solid black line as a function of the characteristic distance for all nonneutron methods: experiments with antiprotonic atoms (antiprotons), measurements of van der Waals (Ederth) and Casimir (Mohideen, Purdue, Lamoreux) forces, and measurements of gravity at short distances (Stanford). Neutron constraints are shown with dashed lines in measurements of the asymmetry of neutron–nucleus scattering (distances $10^{-12}-4\times10^{-7}$ m) and neutron gravitational quantum states ($4\times10^{-7}-10^{-5}$ m). Possible improvements in neutron constraints are shown with dotted lines for measurements of the asymmetry of cold neutron scattering on atoms of inert gases ($10^{-12}-10^{-8}$ m), and precision experiments with quantum states of neutrons in centrifugal ($10^{-8}-10^{-6}$ m) and gravitational ($10^{-6}-10^{-5}$ m) potentials. In the last case, we show the constraint feasible in the flow-through mode at the first stage of this experiment.

as the neutron energy is small enough. Nuclear corrections are also absent because the nuclei are light enough. Therefore, any measured asymmetry in the center-of-mass reference system would imply additional short-range forces.

The presented neutron constraints and competing constraints from experiments studying Casimir and van der Waals forces, as well as antiproton atoms [152, 153], are shown in Fig. 17.

As is clear from Fig. 17, neutron constraints are the most precise in the distance range $2\times10^{-12}-7\times10^{-9}$ m; they could be significantly improved in future experiments. At even larger distances, measurements of Casimir forces and gravity at short distances provide much more stringent constraints than those following from neutron experiments. The most promising neutron experiments in this distance range are precision measurements of gravitational and centrifugal quantum states of neutrons. They could possibly reach a level of interest in the future. We note that an alternative method of setting constraints for additional short-range interactions, the precision measurement of Casimir forces between two parallel plates separated by a distance up to 10 μm [154], is based on experimental methods developed in neutron experiments, in particular, on the absolute precision positioning of the plates [29, 155].

6.2 Constraints on spin-dependent short-range forces

Axions are known as a possible solution to the CP violation problem, and as interesting candidates for explaining dark matter [156]. Axions provide a CP-violating monopole–dipole coupling of spin to matter [157] of the Yukawa type:

$$V(\mathbf{r})=\hbar g_{\mathrm{p}}g_{\mathrm{s}}\,\frac{\boldsymbol{\sigma}\mathbf{n}}{8\pi mc}\left(\frac{1}{\lambda r}+\frac{1}{r^2}\right)\exp\left(-\frac{r}{\lambda}\right), \tag{29}$$

where $g_{\mathrm{p}}g_{\mathrm{s}}$ is the product of couplings at scalar and polarization vertices, λ is the characteristic scale of interaction, r is the distance between the nucleus and the neutron, $\boldsymbol{\sigma}$ is the neutron spin, and $\mathbf{n}=\mathbf{r}/r$ is a unit vector. Additional spin-dependent interactions were classified in a general form in Ref. [158]. Laboratory and astrophysical observations constrain the range for searches by the so-called axion window for distances λ. A comprehensive review of theoretical and experimental activity regarding searches for axions can be found in Ref. [159]. Only a few experiments with magnetized media and a test mass constrain the product $g_{\mathrm{p}}g_{\mathrm{s}}$ in the axion window. One experiment [160] had its peak sensitivity at $\lambda=100$ mm (the axion mass 2 μeV); frequencies of spin precession of Hg^{199} and Cs atoms are compared in it as a function of the test mass in the vicinity of the experimental setup. Another experiment with a macroscopic quality of polarized electrons [161] is most sensitive around $\lambda=10$ mm (the axion mass 20 μeV).

It is clear that the maximum sensitivity of the gravitational experiment is reached at distances close to z_0. We estimate the constraint on the coupling constant. In analogy to the estimate in Section 6.1 (additional interaction (27) between the neutron and the mirror material nuclei resulted in additional potential (28)), a neutron with a given projection of spin on the vertical axis is affected by the additional potential due to interaction (29) between the neutron and the mirror:

$$U(z)=U_0\exp\left(-\frac{z}{\lambda}\right), \tag{30}$$

where

$$U_0=\frac{g_{\mathrm{p}}g_{\mathrm{s}}}{4\pi}\,\frac{\pi\hbar\rho_{\mathrm{m}}\lambda}{2m^2c}\,.$$

This potential would split a gravitational quantum state into two states with opposite spins. Accordingly, the transmission curve for the neutron flux as a function of the size of the slit between the mirror and the scatterer would split as well into two curves with different effective values of the free-fall acceleration. The absence of such a phenomenon for unpolarized neutrons allows constraining the additional interaction as $g_{\mathrm{p}}g_{\mathrm{s}}/(\hbar c)=2\times10^{-15}$ [43, 162, 163]. This constraint could be improved by a factor of $\sim10^3$ in measurements with polarized neutrons in the flow-through mode [164] in the GRANIT spectrometer. The transmission curves for two neutron spin polarizations would be slightly shifted in height in the presence of an additional interaction. The statistical accuracy for measuring such a shift for a reasonable time of about 10 days could reach $\sim10^3$; systematic false effects could be avoided at this precision if paramagnetic impurities on the mirror surface were controlled. The main simplification in the case of spin-dependent short-range forces, compared to the case of spin-independent forces, consists in profiting from relative measurements because the neutron spin can easily be flipped with high

accuracy. In contrast, spin-independent short-range forces cannot be 'switched off,' and therefore absolute measurements should be performed.

A further increase in sensitivity could be achieved in measurements of UCN spin rotation in the vicinity of the surface due to the axion field in installations searching for the neutron electric dipole moment [100, 165], or studying depolarization of UCNs during their reflection from a surface [100, 166]. In both cases, GRANIT is of interest because it combines the statistical sensitivity of competing projects and an option to control systematic effects experimentally by analyzing axion field effects as a function of the distance to the surface. Moreover, the condition of uniformity (smallness) of magnetic fields is relaxed by many orders of magnitude, because relative, not absolute, measurements are needed as a function of the distance to the surface.

6.3 Constraint on the neutron electric charge

With a strong electric field oscillating at the resonance frequency, we can constrain the neutron electric charge by searching for induced transitions between quantum states [43].

Let the mirror be an electrode of a capacitor; an oscillating electric field is applied to it. The perturbation Hamiltonian is then $\hat{V}(t) = e_{\rm n} E \exp(\mathrm{i}\omega t) z$, where $e_{\rm n}$ is the electric charge and E is the electric field strength. The matrix element of this interaction is $F_{\rm n1} = e_{\rm n} E z_{\rm n1}$. The upper limit for the probability of neutron transition to the nth quantum state $P_{\rm lim}$ corresponds to the constraint on the neutron electric charge $e_{\rm n} < [\hbar/(E z_{\rm n1} t)]\sqrt{P_{\rm lim}}$. In an experiment with the electric field strength $E \approx 10^7$ V m^{-1} and the observation time $t \approx 10^3$ s, the upper limit for the transition probability $P_{\rm lim} \approx 10^{-3}$ should be achieved in order to reach the sensitivity corresponding to the current constraint for the neutron electric charge $e_{\rm n} < 10^{-21} e$. The last constraint was measured in the interferometric experiment with very cold neutrons [167]. UCNs were also used for constraining the neutron electric charge [73]. An experiment measuring resonance transitions of neutrons between the quantum states induced by the electric field alone could in principle allow reaching a high sensitivity, but this is not too realistic.

A much better constraint on the neutron electric charge can be obtained by measuring oscillations between highly excited quantum states or using two perturbations (26) simultaneously and measuring the interference between them. Because the sensitivity of such an experiment is apparently defined by parasitic effects (parasitic transitions between quantum states, which cannot yet be precisely taken into account), we calculate the sensitivity later.

6.4 Evolution of localized wave packets

As shown in Section 5.1, UCNs could be elastically and specularly reflected from a surface at least $\sim 10^3$ times; this value greatly increases for small incidence angles. Hence, any kind of quantum mechanical interference or localization would be clearly pronounced. Gravitational quantum states are therefore an excellent laboratory for measuring and studying various quantum mechanical phenomena [16, 17, 168–177]. We consider in more detail the evolution of an initially localized wave packet, which will be used in the GRANIT experiment for measuring the lifetimes of neutrons in quantum states.

The evolution of an initially localized neutron wave packet in the experiment in [27] was analyzed in detail in Refs [171, 177]; an analogous phenomenon for ultracold atoms above an atomic mirror is considered in Ref. [169]. Observation of the evolution of an initially localized wave packet in the GRANIT spectrometer would provide an elegant method to measure lifetimes of neutrons in quantum states. States localized in height expand significantly in the vertical direction in accordance with the eigenstates involved; then they relocalize periodically.

In describing time-dependent solutions of the Schrödinger equation, the concept of overlap integrals $\langle\psi_t|\psi_0\rangle$ for time-dependent quantum states $|\psi_t\rangle$ and initial quantum states $|\psi_0\rangle$ is often used; these integrals are called autocorrelation functions. If a wave packet is described in terms of one-dimensional eigenstates $\psi_n(x)$ with energies E_n as

$$\psi(x,t) = \sum_{n=1}^{\infty} a_n \psi_n(x) \exp\left(-\frac{\mathrm{i}E_n t}{\hbar}\right),$$

where $a_n = \int_{-\infty}^{\infty} \psi_n^*(x)\,\psi(x,t)\,\mathrm{d}x$, then the autocorrelation function can be written as

$$A(t) = \sum_{n=1}^{\infty} |a_n|^2 \exp\left(\frac{\mathrm{i}E_n t}{\hbar}\right).$$

If a localized wave packet is formed by quantum states with close energies (with large values compared to E_1) and the mean value corresponds to the quantum state with a number n_0, then the energies of such quantum states can be expressed as $E_n = E(n)$ by expanding them into a series around the mean value:

$$E(n) \approx E(n_0) + E'(n_0)(n-n_0) + \frac{E''(n_0)}{2!}(n-n_0)^2 + \frac{E'''(n_0)}{3!}(n-n_0)^3 + \ldots .$$

The time dependence of each term in this expansion is evident from

$$\exp\left(\frac{\mathrm{i}E_n t}{\hbar}\right) = \exp(\mathrm{i}\omega_0 t) \exp\left(\frac{\mathrm{i}2\pi(n-n_0)}{T_{\rm cl}}\right) \times \exp\left(\frac{\mathrm{i}2\pi(n-n_0)^2}{T_{\rm rev}}\right) \exp\left(\frac{\mathrm{i}2\pi(n-n_0)^3}{T_{\rm super}}\right),$$

where each term (except for the first one, standing for a common nonobservable phase) defines an important time scale:

$$T_{\rm cl} = \frac{2\pi\hbar}{|E'(n_0)|}, \quad T_{\rm rev} = \frac{4\pi\hbar}{|E''(n_0)|}, \quad T_{\rm super} = \frac{12\pi\hbar}{|E'''(n_0)|} \ldots . \tag{31}$$

A wave packet returns to states close to the initial state periodically, with the characteristic time $T_{\rm rev}$.

To estimate these characteristic times, we consider a neutron in the second quantum state (strictly speaking, such a choice does not satisfy the definition given above, but serves as a start for the following consideration). The classical turning height for this state is $z_2 \approx 24$ μm, the classical period is $T_{\rm cl} = 2\sqrt{2z_2/g} \approx 4.4$ ms, and $T_{\rm rev} = 16 m z_0^2/(\pi\hbar) \approx 46$ ms. Evidently, higher quantum states needed for obtaining revivals require long neutron storage in quantum states; they cannot be achieved in the flow-through

mode but will be reached in the storage mode in the GRANIT spectrometer.

An additional method of identification of periodically localized quantum states is the method of informatics entropy in coordinate and velocity spaces considered in Ref. [175]. This method also works when the use of autocorrelation functions is limited.

6.5 Interaction of neutrons in quantum states with a gravitational field

Neutron gravitational quantum states provide a unique opportunity to study the interaction of a particle in a quantum state with a gravitational field.

6.5.1 Weak equivalence principle for an elementary particle in a quantum state. Quantum states of neutrons in gravitational and centrifugal potentials can be considered the first direct demonstration of the weak equivalence principle of the general relativity for an object (a particle) in a pure quantum state [178–182]. The current accuracy of such a comparison is limited by the precision of the gravitational experiment, but it will be significantly improved in the near future. In the classical case, the weak equivalence principle has been verified with the best accuracy ($\sim 10^{-12}$) using macroscopic bodies [1]. The accuracy of measurements with atoms, $\sim 7 \times 10^{-9}$, [183] is very high as well. Concerning elementary particles, the best accuracy ($\sim 3 \times 10^{-4}$) has been achieved with neutrons [2]. However, a known contradiction occurs in the analysis of another neutron experiment [58], where a gravitationally induced phase shift was measured in a neutron interferometer. As shown in Refs [184, 185], accounting for dynamical diffraction effects in the material (silicon) of the neutron interferometer results in a formal violation of the weak equivalence principle. This statement was followed by a series of more precise experiments [186], where a deviation at the level of $10\,\sigma$ equal to $1.0 \pm 0.1\%$ was also measured. Although the most probable reason for this deviation is apparently some methodical error, an increase in accuracy of neutron experiments by a few orders of magnitude would help clarify the current contradiction. Such an improvement could be achieved in planned experiments with a neutron interferometer of another type [187], or in precision experiments with gravitational quantum states of neutrons in the GRANIT spectrometer.

6.5.2 Noncommutative quantum mechanics. Noncommutative extensions of quantum mechanics, in particular those following from quantum gravity theories, have been discussed for a long time, and most intensively recently. References [188–193] use gravitational quantum states for constraining the model parameters for such extensions. Noncommutative extensions are usually based on the Heisenberg algebra in a d-dimensional space. For gravitational quantum states, the problem reduces to the case where $[x, y] = \mathrm{i}\theta$, $[p_x, p_y] = \mathrm{i}\eta$, and $[x_i, p_j] = \mathrm{i}\hbar_{\mathrm{eff}}\,\delta_{ij}$, $i, j = 1, 2$, with $\hbar_{\mathrm{eff}} = \hbar(1 + \theta\eta/(4\hbar^2))$ [188, 190]. With nonzero noncommutative parameters, the parameters of neutron quantum states would change; this relation allows constraining the parameter η as $\sqrt{\eta} < 0.8$ meV s^{-1}. The hypothetical additional Berry phase caused by noncommutative effects are analyzed in [194], where it is shown that the corresponding effect is proportional to the third power of the small parameter, $\Delta\gamma(S) \sim \eta^3$, where S is the path interval in the noncommutative space.

6.5.3 Nonlinear quantum mechanics. A nonlinear term of the type $-b\psi(x)\ln|\psi(x)|^2$ in the Schrödinger equation due to quantum gravity effects, where b is the nonlinearity constant [195], results in small effects [196, 197]. However, as discussed in Refs [198, 199], under some assumptions, this term can allow a quasi-elastic reflection of a particle from a surface. To avoid any contradiction with known experimental results, the energy change should be extremely small and hence measurable only with UCNs, or perhaps with ultracold atoms. Publication of these studies was also motivated by searches for a solution to the problem of so-called anomalous losses of UCNs from material traps [200]. Experimental verification [201, 202] of the hypothesis of quasi-elastic reflection allowed the authors to constrain the degree of elasticity of UCN reflection from the surface at the level of $\sim 10^{-11}$ eV per collision. Experiments with neutron gravitational quantum states improved the constraints for the probability as well as for the minimum energy transfer by many times [74], with no dedicated measurements. Moreover, it is now possible to study changes in UCN energy per surface collision instead of following integral effects accumulated after many collisions. Furthermore, this constraint is obtained for one component of the neutron velocity. Finally, any hypothetical deviation from standard quantum mechanics should be verified in the purest quantum limit of minimum energies (velocities). We note that the last work is of methodical interest for GRANIT, because highly elastic UCN reflections from a surface are a prerequisite for most of the experiments considered here.

6.5.4 Generalized uncertainty relation. The generalized uncertainty relation occurs naturally in quantum gravity theories and in noncommutative quantum mechanics; it assumes the existence of some characteristic scale $(\Delta x)_{\mathrm{min}}$ that could manifest itself not only at high energies but also in precision experiments at a low energy [203–205]. This parameter is not universal in general, but could depend, for instance, on the mass. Experiments with neutron gravitational quantum states constrain such a scale as $(\Delta x)_{\mathrm{min}} < 2.4$ nm. If we assume that this parameter is universal, then a much stronger constraint can be obtained from measurements of the hydrogen atom spectrum.

6.5.5 Loss of quantum mechanical coherence. Judging by the number of publications on this subject, the fundamental loss of quantum coherence caused by the interaction of a quantum system with a gravitational field [206] has always been of interest. As noted in the first publications [207], neutron interferometric experiments could be sensitive to this phenomenon. The value important for the sensitivity is the time of observation of an interfering system. In the experiment with thermal neutrons in [35], this time was 3×10^{-4} s. In the spectrometer in [34] in the flow-through mode, the observation time reaches 6×10^{-2} s. Measurements of the evolution of an initially localized neutron wave packet, considered in Section 6.4, could also provide a direct estimation of the characteristic time of the fundamental loss of coherence of a quantum system. The observation time in the storage mode in the GRANIT spectrometer will be about 1 s at the fist stage; it could be further increased by a few orders of magnitude. Another method consists in measuring neutron oscillations between two quantum states due to the small mixing interaction (for instance, magnetic). On the other hand, the loss of quantum coherence resulting from the neutron

interaction with a gravitational field (not of a fundamental nature) could be measured in principle if time variations of the gravitational potential are greatly increased locally using the motions of some mass in the vicinity of the installation; simultaneously, resonance quantum transitions should be induced by some other stronger interaction.

6.5.6 Interaction of the neutron spin with a gravitational field. This experiment was considered in the broad context [208–212] of the interaction of the neutron spin with a gravitational field [213–216]. It is shown that spin-dependent corrections are small and hence could not be currently measured.

6.5.7 Gravitational Stark effect. This effect occurs if a gravitating mass is accelerating. Its influence on a particle in such a gravitational field is considered in Ref. [217].

6.5.8 Cosmological consequences. Observation of neutron gravitational quantum states motivated the appearance of theoretical work studying the gravitational quantum particle states of astronomical size [218, 219].

6.5.9 Relativistic corrections, space curvature. Because the UCN velocity is much smaller than relativistic velocities ($v/c \sim 2 \times 10^{-8}$), corresponding corrections to the quantum states are, generally speaking, very small.

Additional information on the interaction of neutrons in gravitational quantum states with a gravitational field could be found, e.g., in Refs [220–226]. The brief review presented in this section covers just the range of scientific interests and competence of the author; it is by no means complete.

6.6 Neutron-tight UCN valve. Extraction of UCNs from an ^{4}He source

Experiments with neutron gravitational quantum states helped in proposing an alternative solution to the problem of a neutron-tight valve for UCN traps; such a valve should operate in the broad temperature range needed for precision neutron lifetime measurements. Current solutions are accompanied by side systematic effects: operation of the gravitational valve [68, 72] deforms the spectrum of stored UCNs (because of the mixing of the UCN spectrum in the rotating trap), and the liquid valve [67, 69–71] uses hydrogen-free Fomblin oil, which leads to intense low heating of UCNs (their quasi-elastic scattering) [76–80]. The principal element of a new proposed neutron valve is two parallel rough plates. Even a macroscopic slit between the plates efficiently reflects UCNs with a probability close to 100% [28, 107, 108].

An analogous process is used to extract UCNs out of an ^{4}He source with minor suppression of the UCN density. We consider the slit between the horizontal mirror and the scatterer above; it transmits UCNs selectively. Let the mirror/scatterer pair be installed at the exit of a UCN trap (or an ^{4}He UCN source). Only neutrons with the vertical angle smaller than some critical value φ_0 bounce on the bottom mirror and pass through the slit [107, 108]. An evident condition for the angle φ_0 is

$$\varphi_0 = \frac{\sqrt{2gz_n}}{V_{\rm hor}}\,, \tag{32}$$

where z_n is the highest open quantum state of neutrons in the slit between the mirror and the scatterer. All neutrons with a larger vertical velocity component scatter back to the trap if their energy is smaller than the critical velocity of the mirror and scatterer. This method could be applied for extracting UCNs from a cryogenic volume of an ^{4}He UCN source. It solves a problem that has existed for many years: that of UCN flow-through extraction from ^{4}He sources with no major suppression of the UCN density in the source. Only neutrons needed for experiments with the GRANIT spectrometer (neutrons with nearly horizontal velocities) leave the ^{4}He volume; other neutrons return to it. Thus, long UCN storage times needed for UCN accumulation could be achieved in the source. The parameters of such a system were optimized in Ref. [108]. The slit length should be ~ 10 cm, the slit height should be $100-200$ μm, the roughness amplitude should be about z_0, and the UCN loss coefficient per bounce should not exceed 10^{-4}.

7. Quantum whispering gallery wave

The whispering gallery effect has been known since ancient times for sound in air [227, 228], later for sound in water, and recently for electromagnetic waves of a broad frequency range: radio, optical, and Roentgen waves [229–232]. This effect consists of wave localization in the vicinity of a concave reflecting surface; it should manifest itself for waves of various natures, in particular, for atoms [233, 234] and neutrons [18, 30, 31, 49, 236]. For material whispering gallery waves, a new quality appears: massive particles are bound into quantum states with the parameters depending on their mass. Mathematically, it can be shown [18, 31] that the problem of such quasistationary neutron states can be solved exactly; it is largely similar to the problem of a particle in an attracting linear potential above a mirror.

Strictly speaking, the results presented in this section are not a review. They have been recently measured, are being analyzed, and will be published in detail later. The essence of the phenomenon is explained in Section 7.1, and prospects for this investigation are formulated in Section 7.2.

7.1 First observation

We consider classical reflection of cold neutrons (Fig. 18) with a velocity $v \sim 10^3$ m s^{-1} (energy $\varepsilon \sim 10^{-2}$ eV) from a

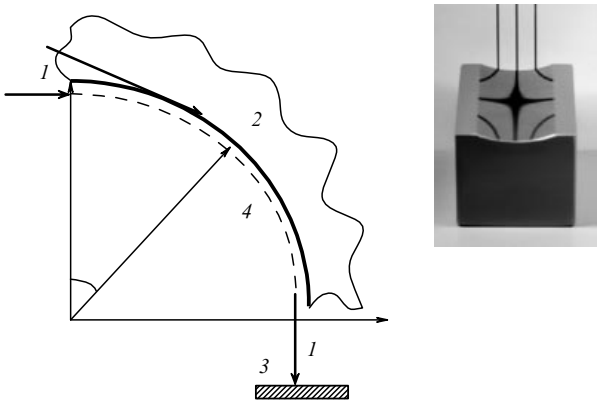

Figure 18. A schematic of an experiment to observe neutron quantum states due to the effective centrifugal potential: *1* — classical neutron trajectories in front of the cylindrical mirror and after scattering on it, *2* — the cylindrical mirror, *3* — the neutron detector, *4* — quantum motion of neutrons along the mirror surface. Inset: a photo of the silicon cylindrical mirror.

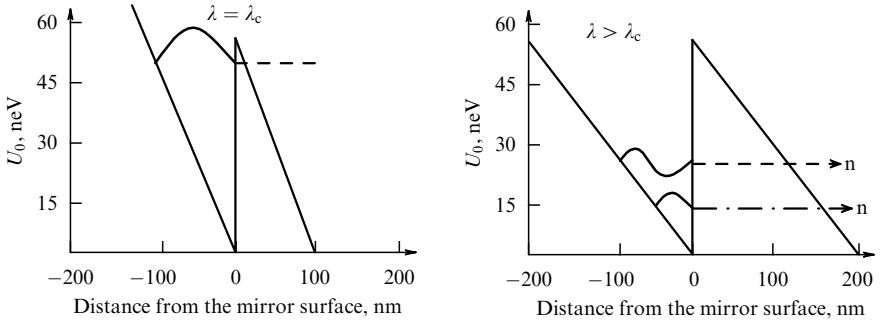

Figure 19. This effective potential appears in the cylindrical reference system. The potential step at the height $z = 0$ is equal to the optical potential U_0 of the mirror material. The derivative of the potential at radial distances $z \neq 0$ is defined by the centrifugal acceleration $a_{\text{centr}} = v^2/R$. Wave functions of the two lowest quantum states ($n = 1, 2$) are shown at heights proportional to their energy. Dashed lines illustrate neutron tunneling through the binding triangle potential.

concave cylindrical mirror with the radius $R = 2.5$ cm (see Ref. [30]). If the energy of neutron radial motion is smaller than the mirror optical potential U_0, the neutron is reflected many times from the mirror at a constant angle as it propagates along the mirror surface. The neutron lifetime on such a trajectory depends on the mirror quality, in particular, on the surface roughness amplitude; the amplitude should not exceed a few angstroms. Because $\varepsilon \gg U_0$, the classically allowed incidence angles φ do not exceed the critical angle $\varphi_c = \sqrt{U_0/\varepsilon} \sim 0.2^\circ$. If the energy of neutron radial motion is larger than the mirror optical potential U_0, the neutron penetrates into the mirror bulk. Tangential and radial motions of reflected neutrons can be separated with a good accuracy both in a classical and in the rigorous quantum mechanical treatment [18, 31]. A reflected neutron experiences the huge centrifugal acceleration $a_{\text{centr}} = v^2/R \sim 10^5 - 10^7 g$. Tangential motion is characterized by the angular momentum with the quantum number $\mu_0 = mvR/\hbar$ with huge characteristic values $\mu_0 = 10^8 - 10^9$; therefore, quantum effects are negligible. In contrast, radial motion is quantized. Quantum states corresponding to the radial motion are formed in the potential well shown in Fig. 19. These are quasistationary states because the probability of neutron tunneling through a bounding triangle potential is never zero, although it can be extremely small for deeply bound states.

A method of studying such quantum states is based on gradually changing the triangle potential well width (see Fig. 19). The width and energy of each quantum state and the number of quantum states in the potential well depend strongly on the neutron velocity v. The width decreases exponentially as v decreases because of the suppression of neutron tunneling through the triangle potential. A smaller value of v corresponds to a broader potential well, and hence to a smaller energy of each state and a larger number of states in the well. We can therefore expect a step-wise dependence of the neutron flux at the exit from the cylindrical mirror as a function of the velocity v. In particular, the flux should increase sharply from zero as the neutron velocity (wavelength) approaches the critical value v_c (λ_c) corresponding to the appearance of the lowest quasistationary state. This value can be estimated using the Heisenberg uncertainty relation $z_{\text{cl}}\sqrt{2mU_0} > 2\pi\hbar$, where $z_{\text{cl}} = RU_0/mv^2$ is the classical maximum distance between the neutron and the mirror. In our case, $\lambda_c \approx 3.9$ Å. The precise value increases weakly as a function of the neutron deviation angle due to neutron tunneling.

Another method of studying such quantum states consists in measuring the distribution of radial neutron velocities using position-sensitive detectors installed at some distance from the mirror. If this distance is large enough, the detection point is uniquely related to the neutron deviation angle defined by the ratio of the radial and tangential velocity components. In particular, if only one quantum state is populated, the distribution of the radial velocity components in this quantum state can be measured directly. Evidently, the most informative and sensitive method consists in simultaneous measurements of radial and tangential velocities. The tangential velocity is measured using the time-of-flight method, and the radial velocity is measured using a position-sensitive detector placed at the distance 3–4 m from the mirror. The first measurements were carried out using a PF1B instrument [236]; the main data were taken using D17 reflectometer [237] at ILL in Grenoble.

The initial width of the neutron beam ($\sim 10^{-4}$ m) was much larger than the characteristic size of the quantum states ($\sim 10^{-7}$ m). The angular divergence in the initial beam was 0.2°. We studied two techniques to populate the quantum states. In the first case, neutrons arrived from the mirror bulk along trajectories tangential to the mirror surface [31]; only a small fraction of such neutrons tunneled into excited quantum states. In the second case, neutrons populated all quantum states from the edge of a truncated cylindrical mirror [18]; here, the fraction of neutrons trapped in quantum states was much higher and the lifetimes of deeply bound quantum states were much larger, and therefore characteristic neutron deviation angles were much larger. A typical result of measurements is shown in Fig. 20.

The pattern corresponding to the quantum states in Fig. 20 is V-shaped. This shape can be explained as follows. The mean deviation angle φ_0 is equal to the angular size of the mirror, i.e., the distribution of radial velocity components is symmetric relative to the zero value. In the case of classical neutron trajectories, the width of the letter V would be proportional to the neutron wavelength λ for any λ because the radial neutron velocity cannot exceed the critical velocity of the mirror material and the letter V would point to $\lambda(\varphi_0) = 0$, as shown in Fig. 20. The evident manifestation of quantum quasistationary states consists in the abrupt appearance of deviated neutrons with the wavelength larger than λ_c; this effect corresponds to the appearance of the lowest state in close analogy to its appearance in experiments with gravitational quantum states [27]. Neutron wavelengths in the vicinity of λ_c

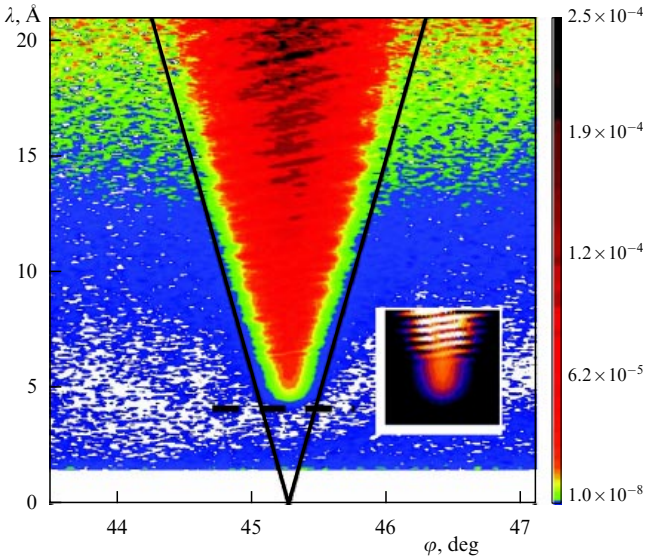

Figure 20. The probability of neutron scattering on a cylindrical mirror is shown in different colors (intensities) as a function of the neutron wavelength λ and the deviation angle φ. Neutrons populate quantum states through a truncated mirror edge. The geometric mirror size is 45.3°. Inclined solid lines indicate the shape for classical trajectories of reflected neutrons. The dashed horizontal line shows the characteristic wavelength λ_c, on which the lowest quantum state appears. Theoretical calculation of the pattern is shown in the inset [30].

correspond to the maximum intensity in the initial neutron spectrum; therefore, the observed threshold phenomenon is particularly convincing. Another manifestation of quantum states consists in the complex structure of interference lines inside the V. The inset in Fig. 20 shows the theoretical pattern simulation; it is similar to the measured pattern in detail. Notably, there is no interference if the wavelength is smaller than ≈ 5.5 Å, because only one quantum state is populated at this wavelength and it has no other state to interfere with. At larger wavelengths, the interference of two quantum states is observed, resulting in a set of equally spaced lines. Further, due to the contributions of many quantum states, the interference picture is more complex. The interference pattern is very sensitive to the potential well shape if near-threshold states are involved; it is not sensitive if only deeply bound states are involved.

7.2 Prospects for using a neutron whispering gallery wave

Evidently, the accuracy achieved in the first experiment ($\sim 10^{-2}$) in estimating quantum parameters can be improved by several orders of magnitude due to a higher precision spectrometry and a broader range of neutron velocities. The current accuracy is not limited by statistics or revealed systematic effects; theoretical analysis has to be developed further.

Deeply bound long-lived quantum states of neutrons in the effective centrifugal potential are a kind of 'precision clock' with well-defined parameters, while near-threshold quantum states are very sensitive to the precise shape of the potential well. The first estimations hold the promise of using this phenomenon for searching for additional short-range forces with a characteristic scale around the quantum state size. On the other hand, such quantum states are useful for studying various phenomena in quantum optics and surface physics, especially for sensitive and precision measurements of surface potential shapes. It is too early to make final conclusions concerning the full range of possible applications.

8. Conclusion

We presented experimental and theoretical results on studies of neutron gravitational quantum states and on applications of this phenomenon and related methods in the physics of particles and fields, in quantum optics, and in surface physics. We briefly noted the first results of studies of the closely related phenomenon of a neutron whispering gallery. The measurement of the near-surface quantum states of these two types is the first direct demonstration of the weak equivalence principle for a massive object in a quantum state. Applications of these phenomena and experimental and theoretical methods of their investigation and precision measurement are currently being intensively developed.

References

1. Su Y et al. *Phys. Rev. D* **50** 3614 (1994)
2. Koester L *Phys. Rev. D* **14** 907 (1976)
3. Zel'dovich Ya B *Zh. Eksp. Teor. Fiz.* **36** 1952 (1959) [*Sov. Phys. JETP* **9** 1389 (1959)]
4. Lushchikov V I et al. *Pis'ma Zh. Eksp. Teor. Fiz.* **9** 40 (1969) [*JETP Lett.* **9** 23 (1969)]
5. Steyerl A *Phys. Lett. B* **29** 33 (1969)
6. Luschikov V I *Phys. Today* **30** (6) 42 (1977)
7. Luschikov V I, Frank A I *Pis'ma Zh. Eksp. Teor. Fiz.* **28** 607 (1978) [*JETP Lett.* **28** 559 (1978)]
8. Fermi E, Marshall L *Phys. Rev.* **71** 666 (1947)
9. Frank A I, Nosov V G *Pis'ma Zh. Eksp. Teor. Fiz.* **79** 387 (2004) [*JETP Lett.* **79** 313 (2004)]
10. Wallis H, Dalibard J, Cohen-Tannoudji C *Appl. Phys. B* **54** 407 (1992)
11. Köhl M, Hänsch T W, Esslinger T *Phys. Rev. Lett.* **87** 160404 (2001)
12. Balykin V I et al. *Phys. Rev. Lett.* **60** 2137 (1988)
13. Kasevich M A, Weiss D S, Chu S *Opt. Lett.* **15** 607 (1990)
14. Aminoff C G et al. *Phys. Rev. Lett.* **71** 3083 (1993)
15. Roach T M et al. *Phys. Rev. Lett.* **75** 629 (1995)
16. Bertolami O, Rosa J G *Phys. Lett. B* **633** 111 (2006)
17. Berberan-Santos M N, Bodunov E N, Pogliani L *J. Math. Chem.* **37** 101 (2005)
18. Nesvizhevsky V V et al. *Phys. Rev. A* **78** 033616 (2008)
19. Breit G *Phys. Rev.* **32** 273 (1928)
20. Gol'dman I I, Krivchenkov V D *Sbornik Zadach po Kvantovoi Mekhanike* (Problems in Quantum Mechanics) (Moscow: Gostekhizdat, 1957); Kogan V I, Galitskii V M *Sbornik Zadach po Kvantovoi Mekhanike* (Problems in Quantum Mechanics) (Moscow: Gostekhizdat, 1956) [Translated into English: Gol'dman I I et al. (Ed. D ter Haar) (New York: Academic Press, 1960)]
21. ter Haar D (Ed.) *Selected Problems in Quantum Mechanics* (New York: Academic Press, 1964)
22. Landau L D, Lifshitz E M *Kvantovaya Mekhanika. Nerelyativistskaya Teoriya* (Quantum Mechanics. Nonrelativistic Theory) (Moscow: Nauka, 1974) [Translated into English (Oxford: Pergamon Press, 1965)]
23. Langhoff P W *Am. J. Phys.* **39** 954 (1971)
24. Flügge S *Practical Quantum Mechanics I* (Berlin: Springer-Verlag, 1974) [Translated into Russian (Moscow: Mir, 1974)]
25. Gibbs R L *Am. J. Phys.* **43** 25 (1975)
26. Sakurai J J *Modern Quantum Mechanics* (Menlo Park, Calif.: Benjamin/Cummings, 1985)
27. Nesvizhevsky V V et al. *Nature* **415** 297 (2002)
28. Nesvizhevsky V V et al. *Phys. Rev. D* **67** 102002 (2003)
29. Nesvizhevsky V V et al. *Eur. Phys. J. C* **40** 479 (2005)
30. Nesvizhevsky V V et al. *Nature Phys.* **6** 114 (2009)
31. Nesvizhevsky V V et al. *New J. Phys.* (2009), submitted

32. Nesvizhevskii V V, Thesis for Doctorate of Physicomathematical Sciences (Moscow: Russian Research Centre 'Kurchatov Institute', 2007)
33. Nesvizhevsky V V, Preprint ILL-96NE14T (Grenoble: Institut Laue – Langevin, 1996)
34. Nesvizhevsky V V et al. *Nucl. Instrum. Meth. Phys. Res. A* **440** 754 (2000)
35. Bowles T J *Nature* **415** 267 (2002)
36. Schwarzschild B *Phys. Today* **55** (3) 20 (2002)
37. Hansson J et al. *Phys. Rev. D* **68** 108701 (2003)
38. Nesvizhevsky V V et al. *Phys. Rev. D* **68** 108702 (2003)
39. Nesvizhevskii V V *Usp. Fiz. Nauk* **173** 102 (2003) [*Phys. Usp.* **46** 93 (2003)]
40. Nesvizhevskii V V *Usp. Fiz. Nauk* **174** 569 (2004) [*Phys. Usp.* **47** 515 (2004)]
41. Nesvizhevsky V V et al., ILL Annual Report-2004 (Eds G Ciconga-ni, C Vettier) (Grenoble: Institut Laue – Langevin, 2004) p. 82
42. Nesvizhevsky V V et al. *J. Res. Natl. Inst. Stand. Technol.* **110** 263 (2005)
43. Nesvizhevsky V V, Protasov K V, in *Trends in Quantum Gravity Research* (Ed. D C Moore) (New York: Nova Sci. Publ., 2006)
44. Abele H et al. *AIP Conf. Proc.* **842** 793 (2006)
45. Voronin A Yu et al. *Phys. Rev. D* **73** 044029 (2006)
46. Meyerovich A E, Nesvizhevsky V V *Phys. Rev. A* **73** 063616 (2006)
47. Adhikari R et al. *Phys. Rev. A* **75** 063613 (2007)
48. Westphal A et al. *Eur. Phys. J. C* **51** 367 (2007)
49. Cubitt R et al. *Nucl. Instrum. Meth. Phys. Res. A* **611** 322 (2009)
50. Baeßler S *J. Phys. G Nucl. Part. Phys.* **36** 104005 (2009)
51. Rooijakkers W et al. *Phys. Rev. A* **68** 063412 (2003)
52. Zabow G, Conroy R S, Prentiss M G *Phys. Rev. Lett.* **92** 180404 (2004)
53. Voronin A Yu, Froelich P *J. Phys. B At. Mol. Opt.* **38** L301 (2005)
54. Voronin A Yu, Froelich P, Zygelman B *Phys. Rev. A* **72** 062903 (2005)
55. Cole M W *Rev. Mod. Phys.* **46** 451 (1974)
56. Freed J H *Ann. Physique* **10** 901 (1985)
57. Longhi S *Phys. Rev. A* **77** 035802 (2008)
58. Colella R, Overhauser A W, Werner S A *Phys. Rev. Lett.* **34** 1472 (1975)
59. Rauch H et al. *Nature* **417** 630 (2002)
60. Ignatovich V K *Fizika Ul'trakholodnykh Neitronov* (The Physics of Ultracold Neutrons) (Moscow: Nauka, 1986) [Translated into English (Oxford: Clarendon Press, 1990)]
61. Golub R, Richardson D J, Lamoreaux S K *Ultra-cold Neutrons* (Bristol: A. Higler, 1991)
62. Pendlebury J M *Annu. Rev. Nucl. Part. Sci.* **43** 687 (1993)
63. Nico J S, Snow W M *Annu. Rev. Nucl. Part. Sci.* **55** 27 (2005)
64. Abele H *Prog. Part. Nucl. Phys.* **60** 1 (2008)
65. Altarev I S et al. *Phys. Lett. B* **276** 242 (1992)
66. Baker C A et al. *Phys. Rev. Lett.* **97** 131801 (2006)
67. Mampe W et al. *Phys. Rev. Lett.* **63** 593 (1989)
68. Nesvizhevskii V V et al. *Zh. Eksp. Teor. Fiz.* **102** 740 (1992) [*Sov. Phys. JETP* **75** 405 (1992)]
69. Mampe W et al. *Pis'ma Zh. Eksp. Teor. Fiz.* **57** 77 (1993) [*JETP Lett.* **57** 82 (1993)]
70. Arzumanov S et al. *Phys. Lett. B* **483** 15 (2000)
71. Pichlmaier A et al. *Nucl. Instrum. Meth. Phys. Res. A* **440** 517 (2000)
72. Serebrov A et al. *Phys. Lett. B* **605** 72 (2005)
73. Borisov Yu V et al. *Zh. Tekh. Fiz.* **58** 951 (1988) [*Sov. Phys. Tech. Phys.* **33** 574 (1988)]
74. Nesvizhevsky V V *Int. J. Mod. Phys. D* **14** 511 (2005)
75. Strelkov A V, Hetzelt M *Zh. Eksp. Teor. Fiz.* **74** 23 (1978) [*Sov. Phys. JETP* **47** 11 (1978)]
76. Nesvizhevsky V V et al. *Yad. Fiz.* **62** 832 (1999) [*Phys. At. Nucl.* **62** 776 (1999)]
77. Nesvizhevsky V V et al. *Eur. J. Appl. Phys* **6** 151 (1999)
78. Geltenbort P et al. *Pis'ma Zh. Eksp. Teor. Fiz.* **70** 175 (1999) [*JETP Lett.* **70** 170 (1999)]
79. Strelkov A V et al. *Nucl. Instrum. Meth. Phys. Res. A* **440** 695 (2000)
80. Bondarenko L N et al. *Yad. Fiz.* **65** 13 (2002) [*Phys. At. Nucl.* **65** 11 (2002)]
81. Strelkov A V *Usp. Fiz. Nauk* **174** 565 (2004) [*Phys. Usp.* **47** 511 (2004)]
82. Steyerl A et al. *Phys. Lett. A* **116** 347 (1986)
83. Jakubek J et al. *Nucl. Instrum. Meth. Phys. Res. A* **600** 651 (2009)
84. Sanuki T et al. *Nucl. Instrum. Meth. Phys. Res. A* **600** 657 (2009)
85. Mezei F *Commun. Phys.* **1** 81 (1976)
86. Schaerpf O *Physica B* **156 – 157** 639 (1989)
87. Gurevich I I, Nemirovskii P E *Zh. Eksp. Teor. Fiz.* **41** 1175 (1961) [*Sov. Phys. JETP* **14** 838 (1962)]
88. Petrillo C et al. *Nucl. Instrum. Meth. Phys. Res. A* **424** 523 (1999)
89. Pignol G, Protasov K, Nesvizhevsky V *Class. Quantum Grav.* **24** 2439 (2007)
90. Nesvizhevsky V V *Nucl. Instrum. Meth. Phys. Res. A* **557** 576 (2006)
91. Nesvizhevsky V V et al.. *Nucl. Instrum. Meth. Phys. Res. A* **578** 435 (2007)
92. Plonka C et al. *Nucl. Instrum. Meth. Phys. Res. A* **578** 450 (2007)
93. Trinks U et al. *Nucl. Instrum. Meth. Phys. Res. A* **440** 666 (2000)
94. Bagrjanov B V et al. *Yad. Fiz.* **62** 844 (1999) [*Phys. At. Nucl.* **62** 787 (1999)]
95. Pokotilovski Yu N *Nucl. Instrum. Meth. Phys. Res. A* **356** 412 (1995)
96. Frank A I, Gähler R *Yad. Fiz.* **63** 605 (2000) [*Phys. At. Nucl.* **63** 545 (2000)]
97. Pignol G et al., arXiv:0708.2541
98. Arminjon M *Phys. Lett. A* **372** 2196 (2008)
99. Morozova V S, Ahmedov B J *Int. J. Mod. Phys. D* **18** 107 (2009)
100. Pignol G, PhD Thesis (Grenoble: ILL/LPSC, 2009)
101. Werner S A, Staudenmann J-L, Colella R *Phys. Rev. Lett.* **42** 1103 (1979)
102. Assoufid L et al. *Proc. SPIE* **5921** 129 (2005)
103. Kreuz M et al. *Nucl. Instrum. Meth. Phys. Res. A* **611** 326 (2009)
104. Felber J et al. *Phys. Rev. A* **53** 319 (1996)
105. Meyerovich A E, Ponomarev I V *Phys. Rev. B* **65** 155413 (2002)
106. Schmidt-Wellenburg P et al. *Nucl. Instrum. Meth. Phys. Res. A* **611** 267 (2009)
107. Schmidt-Wellenburg P et al. *Nucl. Instrum. Meth. Phys. Res. A* **577** 623 (2007)
108. Barnard J, Nesvizhevsky V *Nucl. Instrum. Meth. Phys. Res. A* **591** 431 (2008)
109. Nesvizhevsky V V, Protasov K V, Mackowski J M, Projet Blanc ANR-05-BLAN-0098-01, 2005 – 2009
110. Bondoux D et al. *Nucl. Instrum. Meth. Phys. Res. A* **606** 637 (2009)
111. Arminjon M *Phys. Rev. D* **74** 065017 (2006)
112. Nesvizhevsky V V et al. *Nucl. Instrum. Meth. Phys. Res. A* **595** 631 (2008)
113. Nesvizhevsky V V *Yad. Fiz.* **65** 426 (2002) [*Phys. At. Nucl.* **65** 400 (2002)]
114. Nesvizhevsky V V, Pignol G, Protasov K V *Int. J. Nanosci.* **6** 485 (2007)
115. Mezhov-Deglin L P et al. *J. Low Temp. Phys.* **148** 833 (2007)
116. Mezhov-Deglin L P et al. *J. Low Temp. Phys.* **150** 206 (2008)
117. Boeuf A et al. *Synthetic Met.* **8** 307 (1983)
118. Mattoni C E H et al. *Physica B* **344** 343 (2004)
119. Baker C A et al. *Phys. Lett. A* **308** 67 (2003)
120. Murayama H et al. *Phys. Lett. B* **592** 389 (2004)
121. Arkani-Hamed N, Dimopoulos S, Dvali G *Phys. Lett. B* **429** 263 (1998)
122. Antoniadis I et al. *Phys. Lett. B* **436** 257 (1998)
123. Arkani-Hamed N, Dimopoulos S, Dvali G *Phys. Rev. D* **59** 086004 (1999)
124. Kaluza T *Berl. Ber.* 966 (1921)
125. Klein O *Z. Phys.* **37** 895 (1926)
126. Rubakov V A, Shaposhnikov M E *Phys. Lett. B* **125** 136 (1983)
127. Rubakov V A, Shaposhnikov M E *Phys. Lett. B* **125** 139 (1983)
128. Visser M *Phys. Lett. B* **159** 22 (1985)
129. Antoniadis I *Phys. Lett. B* **246** 377 (1990)
130. Lykken J D *Phys. Rev. D* **54** R3693 (1996)
131. Frank A, Van Isacker P, Gómes-Camacho J *Phys. Lett. B* **582** 15 (2004)
132. Long J C et al. *Nature* **421** 922 (2003)
133. Hewett J, March-Russel J *Phys. Lett. B* **592** 1056 (2004)
134. Gundlach J H *New J. Phys.* **7** 205 (2005)
135. Onofrio R *New J. Phys.* **8** 237 (2006)
136. Kapner D J et al. *Phys. Rev. Lett.* **98** 021101 (2007)
137. Geraci A A et al. *Phys. Rev. D* **78** 022002 (2008)
138. Adelberger E G et al. *Prog. Part. Nucl. Phys.* **62** 102 (2009)

139. Leeb H, Schmiedmayer J *Phys. Rev. Lett.* **68** 1472 (1992)
140. Abele H, Westphal A, ILL Annual Report-2002 (Eds G Cicongani, C Vettier) (Grenoble: Institut Laue – Langevin, 2004) p. 76
141. Bertolami O, Nunes F M *Class. Quantum Grav.* **20** L61 (2003)
142. Abele H, Baeßler S, Westphal A *Lecture Notes Phys.* **631** 355 (2003)
143. Nesvizhevsky V V, Protasov K V *Class. Quantum Grav.* **21** 4557 (2004)
144. Nesvizhevsky V V, Protasov K V *J. Res. Natl. Inst. Stand. Technol.* **110** 269 (2005)
145. Zimmer O, Kaiser N *Class. Quantum Grav.* **23** 6077 (2006)
146. Nesvizhevsky V V, Protasov K V *Class. Quantum Grav.* **23** 6081 (2006)
147. Greene G L, Gudkov V *Phys. Rev. C* **75** 015501 (2007)
148. Nesvizhevsky V V, Pignol G, Protasov K V *Phys. Rev. D* **77** 034020 (2008)
149. Kamyshkov Yu, Tithof J, Vysotsky M *Phys. Rev. D* **78** 114029 (2008)
150. Buisseret F, Silvestre-Brac B, Mathieu V *Class. Quantum Grav.* **24** 855 (2007)
151. Fermi E "A course in neutron physics", in *Collected Papers* Vol. 2 (Chicago: Univ. of Chicago Press, 1965) [Translated into Russian (Moscow: Nauka, 1972)]
152. Hori M et al. *Phys. Rev. Lett.* **91** 123401 (2003)
153. Korobov V I *Phys. Rev. A* **67** 062501 (2003)
154. Lambrecht A et al. *Class. Quantum Grav.* **22** 5397 (2005)
155. Schrauwen J, Diploma Thesis (Gent: Univ. of Gent, 2004)
156. Kolb E W, Turner M *The Early Universe* (Redwood, Mass.: Addison-Wesley, 1990)
157. Moody J E, Wilczek F *Phys. Rev. D* **30** 130 (1984)
158. Dobrescu B A, Mocioiu I *J. High Energy Phys.* (11) 005 (2006)
159. Murayama H et al. *Phys. Lett. B* **592** 389 (2004)
160. Youdin A N et al. *Phys. Rev. Lett.* **77** 2170 (1996)
161. Ni W-T et al. *Phys. Rev. Lett.* **82** 2439 (1999)
162. Baeßler S et al. *Phys. Rev. D* **75** 075006 (2007)
163. Baeßler S et al. *Phys. Lett. B* **667** 1 (2008)
164. Baeßler S et al. *Nucl. Instrum. Meth. Phys. Res. A* **611** 149 (2009)
165. Zimmer O, arXiv:0810.3215
166. Serebrov A P *Phys. Lett. B* **680** 423 (2009); arXiv:0902.1056
167. Baumann J et al. *Phys. Rev. D* **37** 3107 (1988)
168. Onofrio R, Viola L *Phys. Rev. A* **53** 3773 (1996)
169. Gea-Banacloche J *Am. J. Phys.* **67** 776 (1999)
170. Kälbermann G *J. Phys. A Math. Gen.* **35** 9829 (2002)
171. Robinett R W *Phys. Rep.* **392** 1 (2004)
172. Belloni M, Doncheski M A, Robinett R W *Phys. Scripta* **72** 122 (2005)
173. Mather W H, Fox R F *Phys. Rev. A* **73** 032109 (2006)
174. Witthaut D, Korsch H J *J. Phys. A Math. Gen.* **39** 14687 (2006)
175. Romera E, de los Santos F *Phys. Rev. Lett.* **99** 263601 (2007)
176. González G *Rev. Mexic. Fis.* **54** 5 (2008)
177. Belloni M, Robinett R W *J. Phys. A Math. Theor.* **42** 075203 (2009)
178. Viola L, Onofrio R *Phys. Rev. D* **55** 455 (1997)
179. Herdegen A, Wawrzycki J *Phys. Rev. D* **66** 044007 (2002)
180. Ahluwalia D V *Mod. Phys. Lett. A* **17** 1135 (2002)
181. Chryssomalakos C, Sudarsky D *Gen. Relat. Grav.* **35** 605 (2003)
182. Wawrzycki J *Acta Phys. Polon. B* **35** 613 (2004)
183. Peters A, Chung K Y, Chu S *Nature* **400** 849 (1999)
184. Bonse U, Wroblewski T *Phys. Rev. D* **30** 1214 (1984)
185. Horne M A *Physica B+C* **137** 260 (1986)
186. Littrell K C, Allman B E, Werner S A *Phys. Rev. A* **56** 1767 (1997)
187. Frank A I et al. *Pis'ma Zh. Eksp. Teor. Fiz.* **86** 255 (2007) [*JETP Lett.* **86** 225 (2007)]
188. Bertolami O et al. *Phys. Rev. D* **72** 025010 (2005)
189. Bertolami O et al. *Mod. Phys. Lett. A* **21** 795 (2006)
190. Banerjee R, Roy B D, Samanta S *Phys. Rev. D* **74** 045015 (2006)
191. Saha A *Eur. Phys. J. C* **51** 199 (2007)
192. Giri P R, Roy P *Eur. Phys. J. C* **57** 835 (2008)
193. Giri P R, Roy P *Eur. Phys. J. C* **60** 157 (2009)
194. Bastos C, Bertolami O *Phys. Lett. A* **372** 5556 (2008)
195. Weinberg S *Phys. Rev. Lett.* **62** 485 (1989)
196. Bertolami O *Phys. Lett. A* **154** 225 (1991)
197. Bollinger J J et al. *Phys. Rev. Lett.* **63** 1031 (1989)
198. Steyerl A, Malik S S *Ann. Physics* **217** 222 (1992)
199. Steyerl A, Malik S S *Phys. Lett. A* **217** 194 (1996)
200. Alfimenkov V P et al. *Pis'ma Zh. Eksp. Teor. Fiz.* **55** 92 (1992) [*JETP Lett.* **55** 84 (1992)]
201. Steyerl A et al. *J. Physique III* **7** 1941 (1997)
202. Bestle T et al. *Phys. Lett. A* **244** 217 (1998)
203. Brau F, Buisseret F *Phys. Rev. D* **74** 036002 (2006)
204. Ahluwalia-Khalilova D V *Int. J. Mod. Phys. D* **14** 2151 (2005)
205. Panella O *Phys. Rev. D* **76** 045012 (2007)
206. Hawking S W *Commun. Math. Phys.* **87** 395 (1982)
207. Ellis J et al. *Nucl. Phys. B* **241** 381 (1984)
208. Kobzarev I Yu, Okun' L B *Zh. Eksp. Teor. Fiz.* **43** 1904 (1962) [*Sov. Phys. JETP* **16** 1343 (1963)]
209. Leitner J, Okubo S *Phys. Rev.* **136** B1542 (1964)
210. Mashhoon B *Class. Quantum Grav.* **17** 2399 (2000)
211. Obukhov Yu N *Phys. Rev. Lett.* **86** 192 (2001)
212. Bini D, Cherubini Ch, Mashhoon B *Class. Quantum Grav.* **21** 3893 (2004)
213. Silenko A J, Teryaev O V *Phys. Rev. D* **76** 061101(R) (2007)
214. Boulanger N, Spindel Ph, Buisseret F *Phys. Rev. D* **74** 125014 (2006)
215. Alimohammadi M, Vakili B *Ann. Physics* **310** 95 (2004)
216. Leclerc M *Class. Quantum Grav.* **22** 3203 (2005)
217. Bini D, Cherubini C, Mashhoon B *Phys. Rev. D* **70** 044020 (2004)
218. Ernest A D *J. Phys. A Math. Theor.* **42** 115207 (2009)
219. Ernest A D *J. Phys. A Math. Theor.* **42** 115208 (2009)
220. Kiefer C, Weber C *Ann. Physik* **14** 253 (2005)
221. Khorrami M, Alimohammadi M, Shariati A *Ann. Physics* **304** 91 (2003)
222. Wu N *Commun. Theor. Phys.* **45** 452 (2006)
223. Accioly A, Blas H *Mod. Phys. Lett. A* **22** 961 (2007)
224. Mann R B, Young M B *Class. Quantum Grav.* **24** 951 (2007)
225. Alimohammadi M, Baghjary A A *Int. J. Mod. Phys. A* **23** 1613 (2008)
226. Arminjon M *Found. Phys.* **38** 1020 (2008)
227. Strutt J W (Baron Rayleigh) *The Theory of Sound* Vol. 2 (London: Macmillan, 1878) [Translated into Russian (Moscow: Gostekhizdat, 1955)]
228. Rayleigh (Lord) *Philos. Mag.* **27** 100 (1914)
229. Mie G *Ann. Physik* **330** 377 (1908), volume number is indicated in accordance with the uniform numbering of volumes introduced by Wiley InterScience online; in the original, the volume number is 25
230. Debye P *Ann. Physik* **335** 57 (1909), volume number is indicated in accordance with the uniform numbering of volumes introduced by Wiley InterScience online; in the original, the volume number is 30
231. Oraevsky A N *Kvantovaya Elektron.* **32** 377 (2002) [*Quantum Electron.* **32** 377 (2002)]
232. Vahala K J *Nature* **424** 839 (2003)
233. Mabuchi H, Kimble H J *Opt. Lett.* **19** 749 (1994)
234. Vernooy D W, Kimbl H J *Phys. Rev. A* **55** 1239 (1997)
235. Watson P J S *J. Phys. G Nucl. Part. Phys.* **29** 1451 (2003)
236. Abele H et al. *Nucl. Instrum. Meth. Phys. Res. A* **562** 407 (2006)
237. Cubitt R, Fragneto G *Appl. Phys. A* **74** S329 (2002)